Benchmarking Data-Driven Rainfall-Runoff Models in Great Britain: A comparison of LSTM-based models with four lumped conceptual models

Thomas Lees[1], Marcus Buechel[1], Bailey Anderson[1], Louise Slater[1], Steven Reece[2], Gemma Coxon[3], and Simon J. Dadson[1,4]

[1]School of Geography and the Environment, University of Oxford, South Parks Road, Oxford, United Kingdom, OX1 3QY
[2]Department of Engineering, University of Oxford, Oxford, United Kingdom
[3]Geographical Sciences, University of Bristol, Bristol, United Kingdom
[4]UK Centre for Ecology and Hydrology, Maclean Building, Crowmarsh Gifford, Wallingford, United Kingdom, OX10 8BB

Correspondence: Thomas Lees (thomas.lees@chch.ox.ac.uk)

Abstract. Long Short-Term Memory models (LSTMs) are recurrent neural networks from the field of Deep Learning (DL) which have shown promise for time-series modelling, especially in conditions when data are abundant. Previous studies have demonstrated the applicability of LSTM based models for rainfall-runoff modelling, however, LSTMs have not been tested on catchments in Great Britain (GB). Moreover, opportunities exist to use spatial and seasonal patterns in model performances to improve our understanding of hydrological processes, and to examine the advantages and disadvantages of LSTM-based models for hydrological simulation. By training two LSTM architectures across a large sample of 669 catchments in GB, we demonstrate that the LSTM and the Entity Aware LSTM (EA LSTM) simulate discharge with median NSE scores of 0.88 and 0.86 respectively. We find that the LSTM based models outperform a suite of benchmark conceptual models, suggesting an opportunity to use additional data to refine conceptual models. In summary, the LSTM based models show the largest performance improvements in the North East of Scotland and in South East England. The South East of England remained difficult to model however, in part due to the inability of the LSTMs configured in this study to learn groundwater processes, human abstractions and complex percolation properties from the hydro-meteorological variables typically employed for hydrological modelling.

1 Introduction

Rainfall-runoff models have evolved over many decades, reflecting a diversity of applications and purposes. These models range from physically based, spatially explicit models such as SHETRAN (Birkinshaw et al., 2010), CLASSIC (Crooks et al., 2014) and PARFLOW (Maxwell et al., 2009) to lumped conceptual models, such as TOPMODEL (Beven and Kirkby, 1979) and VIC (Liang, 1994). Additionally, data-driven models have also been used for modelling rainfall-runoff processes (Reich-

stein et al., 2019; Elshorbagy et al., 2010; Wilby et al., 2003; Nourani et al., 2014; Le et al., 2019; Gauch et al., 2021b). The diversity of modelling approaches reflects the diversity of user objectives, uncertainty in terms of how to best represent the stores and fluxes of water and energy and the trade-offs in terms of data requirements, degree of realism and computational costs (Beven, 2011).

Data-driven models range from simple regression models to large neural networks with thousands of parameters. These methods draw on empirical relationships between inputs and outputs to form a representation of how the hydrological system operates more generally (Beven, 2011). Other approaches from the class of data-driven models, such as statistical modelling and machine learning include genetic programming (Chadalawada et al., 2020; Herath et al., 2020), random forests (Booker and Woods, 2014) and support vector regression models (Elshorbagy et al., 2010). Alternative empirical approaches also exist, including data-based mechanistic (DBM) modelling (Young, 1998, 2003). DBM approaches suggest that rather than imposing model structures from the outset, hydrologists should in the first instance allow the data to suggest an appropriate model structure. Then, the modeller should see if there is a mechanistic interpretation of the learned model structure (Young and Beven, 1994). Our modelling approach uses Deep Learning (DL) techniques, which have produced accurate predictions on a wide variety of tasks, including rainfall-runoff modelling (Huntingford et al., 2019), and represent a fruitful area of further exploration for hydrologists and Earth scientists (Reichstein et al., 2019). For a more complete picture on the uses of DL techniques in hydrology, an interested reader is referred to Shen (2018); Beven (2020); Nearing et al. (2020b); Kratzert et al. (2018).

DL methods have been used in hydrology and meteorology for decades (Daniell, 1991; Halff et al., 1993; Dawson and Wilby, 1998; Wilby et al., 2003; Peel and McMahon, 2020). However, one architecture explicitly designed for time-series simulation, the Long Short-Term Memory network (LSTM) (Hochreiter et al., 2001; Hochreiter, 1991), has recently demonstrated credible performance for modelling hydrological signatures across the Continental United States (CONUS) (Kratzert et al., 2018, 2019; Duan et al., 2020; Feng et al., 2020; Gauch et al., 2021b; Fang et al., 2018, 2020). More recent work has begun not only to explore the accuracy of forecasts, but also to use LSTMs to: (i) provide estimates of uncertainty (Klotz et al., 2020); (ii) explore the ability of the LSTM to integrate prior physical knowledge into DL model architectures (Hoedt et al., 2021; Jiang et al., 2020); and (iii) use LSTMs to produce predictions at multiple timescales from a single model (Gauch et al., 2021a).

By contrast with the physically-based, spatially-explicit hydrological models, lumped conceptual models have relatively few parameters and simulate the stores and fluxes of water on a catchment scale, for example, using a single store to represent the catchment-wide upper-soil water storage (Beven, 2011). Lumped conceptual models have lower data and computational requirements when compared to the spatially-explicit, physically-based, models, which is one reason they are often used for operational purposes (Clark et al., 2008). There exist many lumped conceptual models, differing in their internal structures, the equations that govern fluxes of water and energy, and the processes that are included (Knoben et al., 2019). As an evidence-guided discipline, performance benchmarks provide hydrologists with an objective means for selecting between different models, instead of model selection by lineage or affiliation (Addor and Melsen, 2019). Furthermore, when applied over a large sample of catchments, differences in model performance can be instructive with regards to the hydrological conditions that are well simulated by one model compared with others (Gupta et al., 2014). Increasingly, "we need large-scale evaluations of

model capability to identify which processes are important and which model structure(s) are most appropriate" (Lane et al., 2019, p4012).

This paper seeks to address three research gaps. First, there exists no large-sample performance benchmark of LSTMs in a GB context. This is important because scientists and practitioners are interested in using LSTMs as hydrological models for hazard impact assessment, hazard early warning and rainfall-runoff modelling (Shen, 2018). Therefore, a rigorous assessment of LSTM performances is necessary to determine whether such a model choice is appropriate in the GB context. Furthermore, given that the data archives are rich in GB, there exists a very good opportunity to learn more about the capabilities and limitations of LSTM-based methods (Clark and Khatami, 2021). Second, there exists only one other comparison of the EA LSTM performance against the LSTM (Kratzert et al., 2019). Finally, there exist no studies that explore the relationship of performance differences (between conceptual and deep learning models) with the hydrological conditions in which those differences occur. The aim of studying the relationship between performance differences and hydrological conditions is to determine how best to improve our conceptual models. What information might be present in the underlying data that can help identify processes that are currently missing from our conceptual models?

The research questions that this study seeks to address are determined by the research gaps identified above.

1. How well do LSTM-based models (including the EA LSTM) simulate discharge in Great Britain?

2. How do LSTM-based model performances compare with the conceptual models used as a benchmark?

3. Can we extract information from the spatial and temporal patterns in diagnostic measures? e.g. What is the relationship between LSTM performance and catchment attributes?

To address these questions, we have trained an ensemble of 8 LSTMs and 8 EA LSTMs on 669 catchments in Great Britain. We compare the results of the LSTM models with four deterministic lumped-conceptual models from a previous benchmarking study (Lane et al., 2019). This paper provides an evaluation of LSTM model ability across a large sample of GB catchments. We explore the association between catchment characteristics and the differences in model performances and present a data-driven benchmark that reflects the null-hypothesis of what information is present in a large sample dataset (Nearing et al., 2020b). Future modelling efforts may seek to assess whether hydrological theories encoded in conceptual and process-based models may contain more information than the benchmarks provided here (Nearing et al., 2020a).

We believe that the research addresses the following needs of the hydrological community: (i) practitioners wishing to know whether the LSTM is a justifiable model choice in the GB context, (ii) scientists and practitioners interested in understanding under what hydrological conditions (e.g. catchment attributes) the LSTM performance differs from conceptual models, and (iii) as a reference for future GB-wide modelling studies.

2 Methods

2.1 Data - CAMELS GB

All data employed in this analysis originate from the CAMELS-GB data (Coxon et al., 2020a). CAMELS-GB is a recently-released, large-sample, long-term, daily data set that offers the potential for GB-wide modelling studies. CAMELS-GB collates hydrologically relevant data for 671 GB catchments between the years of 1970 and 2015. The data set includes daily time series for meteorology (dynamic data - $\mathbf{X_{t,n}}$); and discharge (target data - $\mathbf{y_{t,n}}$). Also included are catchment attributes (static data, $\mathbf{A_{t,n}}$) such as topography, climate, hydrologic signatures, soil and land cover, hydrogeology, and human influence. These features are, in reality, not static over time. However, for the purposes of this study we treat these features as time-invariant. Further information on the variables we used as input to our model can be found in Table 1. The reader is directed to Coxon et al. (2020b) for details of the source of the data, how the data were processed and a discussion of data limitations.

The data set contains novel inputs compared with previous CAMELS (US, Chile, Brazil) data sets (Addor et al., 2017; Alvarez-Garreton et al., 2018; Chagas et al., 2020), such as human attributes, calculated potential evapotranspiration (pet) and uncertainty estimates. We do not use all of these features here. The static attributes we use to train the LSTM models are listed in Table 1. These static attributes were chosen to reproduce the experimental framework of Kratzert et al. (2019), however, the differences reflect the fact that the CAMELS-US and CAMELS-GB have slightly different attributes. These include both catchment properties and climate properties, describing the conditions relevant for rainfall-runoff modelling in different catchments.

2.2 An Overview of the LSTM and EALSTM

In this paper, we test two neural network architectures used in other hydrological studies (Shen et al., 2018; Kratzert et al., 2019). The first is the LSTM, which has been used in a variety of time-series modelling applications. The second model is the EA LSTM, which conditions the discharge response to meteorological forcings on time-invariant properties of river catchments, such as soil and topographic attributes, treating these time-invariant properties separately. For a summary of notation used throughout the paper please refer to Table 2:

What follows is a brief introduction to the LSTM model architectures. For a more complete description of these models please refer to Appendix A and Kratzert et al. (2018, 2019).

The LSTM has a strong inductive bias towards retaining information over long sequences (Hochreiter, 1991; Bengio et al., 1994). This means that the LSTM architecture is designed to retain information that is important over both long and short term time horizons. LSTMs do this by maintaining two state vectors, a cell memory vector that captures slowly evolving processes ($\mathbf{C_t}$) and a more quickly evolving state vector, colloquially named the "hidden" vector ($\mathbf{h_t}$). Information flow is controlled by a series of 'gates' which are neural network layers that determine what information is removed from $\mathbf{f_t}$ (forget gate), what information is stored in $\mathbf{i_t}$ (input gate) and what information is passed to the $\mathbf{o_t}$ (output gate) respectively.

The Entity Aware Long Short-Term Memory (EA LSTM) modifies the forget gate, so that the output of the forget gate is a function of only the static catchment attributes ($\mathbf{A_n}$) rather than both the catchment attributes and the dynamic data

Table 1. Catchment attributes from the CAMELS-GB data set (Coxon et al., 2020b) used to train the LSTM based models, the static features included in A.

Static Variables	Static Variable Description	Median	Range
area	catchment area (km^2)	152	[2, 9931]
elev_mean	mean elevation (m a.s.l)	163	[25, 682]
dpsbar	slope of the catchment mean drainage path (mkm^{-1})	79	[12, 488]
sand_perc	percent sand (%)	43	[19, 82]
silt_perc	percent silt (%)	30	[9, 43]
clay_perc	percent clay (%)	24	[7, 51]
porosity_hypres	soil porosity calculated using the hypres pedotransfer function (-)	47	[34, 81]
conductivity_hypres	hydraulic conductivity calculated using the hypres pedotransfer function (cmh^{-1})	1	[0.5, 3]
soil_depth_pelletier	depth to bedrock (m)	1	[0.5, 42]
frac_snow	fraction of precipitation falling as snow (for days colder than 0°C)	0.02	[0.00, 0.17]
dwood_perc	percent of catchment that is deciduous woodland (%)	6	[0, 37]
ewood_perc	percent of catchment that is evergreen woodland (%)	2	[0, 93]
crop_perc	percent of catchment that is cropland (%)	13	[0.00, 91]
urban_perc	percent of catchment that is urban area (%)	3	[0.00, 81]
reservoir_cap	catchment reservoir capacity (ML)	0	[0, 8 x 10^7]
p_mean	mean daily precipitation ($mm\,day^{-1}$)	2.57	[1.54, 9.61]
pet_mean	mean daily PET ($mm\,day^{-1}$)	1.38	[1.03, 1.51]
p_seasonality	seasonality and timing of precipitation (estimated using sine curves)	-0.14	[-0.42, 0.14]
high_prec_freq	frequency of high-precipitation days ($\geq$ 5x mean daily precipitation)	15.69	[7.58, 20.73]
low_prec_freq	frequency of dry days (< 1 $mm\,day^{-1}$)	214.23	[1.63, 259.23]
high_prec_dur	average duration of high-precipitation events ($\geq$ 5x mean daily precipitation)	1.14	[1.05, 1.25]
low_prec_dur	average duration of dry periods (number of consecutive days < 1 $mm\,day^{-1}$)	3.70	[2.64, 4.67]

($[\mathbf{X_{t,n}}, \mathbf{A_n}]$). The EA LSTM was developed specifically for rainfall-runoff modelling (Kratzert et al., 2019). For the sake of clarity, it is important to note that both models receive the same information. The LSTM still receives the static catchment attributes. However, rather than affecting only the input gate, the static data can influence all gates, since they are appended to a vector of dynamic inputs ($[\mathbf{X_{t,n}}, \mathbf{A_n}]$) and so the same information is given to the LSTM at each timestep. The static attributes are used by the LSTM in the same way as the dynamic data. This offers extra flexibility for the LSTM compared with the EA LSTM, since the LSTM is able to modify the input gate based on information from time-varying data, whereas the EA LSTM is not. We are using the static nature of the data as a constraint on the EA LSTM to reflect the nature of the input data (separated into static and dynamic inputs).

Table 2. Table describing the notation used throughout the paper.

Symbol	Description	Notes
$\mathbf{y_{t,n}}$	Our target variable, specific discharge at time t, catchment n	$\mathrm{mm\,day^{-1}}$
$\hat{\mathbf{y}}_{\mathbf{t,n}}$	Simulated specific discharge at time t, catchment n, predicted by the model $\mathrm{M}_{\boldsymbol{\theta}}$	$\mathrm{mm\,day^{-1}}$
n	Gauge ID	-
$\mathrm{p}_{t,n}$	Precipitation	$\mathrm{mm\,day^{-1}}$
$\mathrm{pet}_{t,n}$	Potential evapotranspiration	$\mathrm{mm\,day^{-1}}$
$\mathrm{T}_{t,n}$	Temperature	$^\circ\mathrm{C}$
$\mathbf{A_n}$	Catchment attributes (static data)	
$\mathbf{X_{t,n}}$	Hydro-meteorological data (dynamic data)	$\left[\mathrm{p}_{t,n}, \mathrm{pet}_{t,n}, \mathrm{t}_{t,n}\right]$
hs	Hidden size	$\mathrm{hs} = 64$
$\mathbf{W}_{\mathrm{layer}}$	The matrix of learnable weights	-
b_{layer}	The vector of learnable biases	-
$\boldsymbol{\theta}$	Learned model parameters, representing all $\mathbf{W}_{\mathrm{layer}}$ and $\mathbf{b}_{\mathrm{layer}}$	-
$\mathrm{M}_{\boldsymbol{\theta}}$	The model (LSTM or EA LSTM) with parameters $\boldsymbol{\theta}$	-
$\mathbf{C_t}$	The cell state of the LSTM models.	$\mathbb{R}^{\mathrm{hs}}$
$\tilde{\mathbf{C}}_{\mathbf{t}}$	The candidate cell state values	$\tilde{\mathbf{C}}_{\mathbf{t}} \in \mathbb{R} \mid -1 < x < 1\}$
$\mathbf{h_t}$	The hidden state of the LSTM models.	$\mathbb{R}^{\mathrm{hs}}$
$\mathbf{f_t}$	The forget gate of the LSTM models	$\{\mathbf{f_t} \in \mathbb{R} \mid 0 < x < 1\}$
$\mathbf{i_t}$	The input gate of the LSTM models	$\{\mathbf{i_t} \in \mathbb{R} \mid 0 < x < 1\}$
$\mathbf{o_t}$	The output gate of the LSTM models	$\{\mathbf{o_t} \in \mathbb{R} \mid 0 < x < 1\}$
ℓ	The Loss Function used to train the model (Nash Sutcliffe Efficiency)	-

2.3 Model Training

We used the "neuralhydrology" codebase, written in Python 3.6 (Van Rossum et al., 2007), to train and evaluate the models, found here: github.com/neuralhydrology/neuralhydrology/. The configuration files used to run the models can be found using the links at the end of this article. The predictions and error metrics for the fitted models can be found online at Zenodo (zenodo.org/record/4555820, last accessed: 19 July 2021).

The goal of rainfall-runoff modelling is to predict time-varying specific discharge, $\mathbf{y_n} = (\mathbf{y_{1,n}}, ..., \mathbf{y_{T,n}}) \in \mathbb{R}^T$ (mm day^{-1}) for time $t = \{1, ..., T\}$ at measuring gauge n of N, given hydro-meteorological forcing data, $\mathbf{X_n} = (\mathbf{X_{1,n}}, ..., \mathbf{X_{T,n}})$, and catchment attributes ($\mathbf{A_n}$ - Table 1) within the catchment area upstream of the gauge. In the present case for GB, $N = 669$. Although the underlying CAMELS-GB data has 671 station gauges, we trained on data from only 669 stations because two basins have missing data in the static attributes; stations 18011 and 26006 have missing mean elevation (elev_mean) and mean drainage path slope (dpsbar).

Our task is to train a regional hydrological model, i.e. one model for all catchments in the dataset. This means that we learn a single set of parameters, $\boldsymbol{\theta}$, of a model, M_θ, that minimizes the loss function, $\ell(\hat{\mathbf{y}}_{\mathbf{t,n}}, \mathbf{y_n})$, for all flow gauges, and thus accurately simulates discharge ($\hat{\mathbf{y}}_{\mathbf{t,n}}$) for all of the basins in our subset of CAMELS-GB:

$$\hat{\mathbf{y}}_{\mathbf{t,n}} = \mathrm{M}_\theta \left([\mathbf{A_n}, \mathbf{X_{t-k+1,n}}, \ldots, \mathbf{X_{t,n}}] ; \boldsymbol{\theta} \right) \tag{1}$$

140   We train our model using the Nash Sutcliffe Efficiency (NSE) loss as our objective function (ℓ), as described in Kratzert et al. (2019). Other objective functions could be used, however, we use the same objective function as the conceptual models we compare against, in order to control the possible sources of performance differences. The NSE describes the squared error loss normalized by the total variance of the observations. In order to account for the fact that some basins will have lower variance than others, we follow Kratzert et al. (2019) to normalize by basin-specific variance. This prevents the loss from being overly 145   weighted towards high-variance catchments.

    For this study we trained the models on the days from 1 January 1988 to 31 December 1997 and tested on a hold-out sample using the days from 1 January 1998 to 31 December 2008 (4018 days of test data). We withheld the years 1975 to 1980 from the training process to check the performance of the model during training (our validation set). This means that we have separate time periods for calibration (1988–1997; train period), and evaluation (1998–2008; hold-out test period). These train and test 150   periods were chosen to facilitate the comparison with the study whose published results for four lumped hydrological models we use as a benchmark (Lane et al., 2019). For further analysis of the train and test periods please see Appendix B.

    Our input data were taken from CAMELS-GB, described above (Coxon et al., 2020b). We used precipitation, potential evapotranspiration and temperature as dynamic inputs ($\mathbf{X_{t,n}} = \left[\mathrm{p}_{t,n}, \mathrm{pet}_{t,n}, \mathrm{T}_{t,n} \right]$). We selected 21 individual features describing each catchment's topographic, soil, land-cover, and climatic properties as static inputs ($\mathbf{A_n}$). These attributes were 155   chosen to reflect hydrological information that the model can use to distinguish between catchment rainfall-runoff behaviours (Kratzert et al., 2019). These catchment attributes are described in Table 1. For both LSTM models we pass the final hidden output through a fully connected (linear) layer. This final layer maps our hidden state vector to a scalar prediction ($\hat{\mathbf{y}}_{\mathbf{t,n}} \in \mathbb{R}$) for discharge at that gauge on that day. We give the models one year of daily dynamic data (365 input timesteps, $X_n = [\mathbf{X_{t-365,n}}, \ldots, \mathbf{X_{t,n}}]$) to predict the final timestep of specific discharge ($\hat{\mathbf{y}}_{\mathbf{t,n}}$).

160   All national results shown below are calculated for the 518 gauges that are found in both the CAMELS GB data and the benchmark data. We then evaluate model performance on all of these basins for our test (evaluation) period (1998–2008). For each model (LSTM, EA LSTM) we also calculate the average of an ensemble of eight individually-trained models with different random seeds. This strategy accounts for the random initialisation of the network and the stochastic nature of the optimisation algorithm. We used a hidden size (hs) of 64 and a final fully connected layer with a dropout rate of 0.4, which 165   aims to avoid overfitting. Dropout works by randomly forcing certain weights in the network to zero ("dropping them out"), forcing the remaining weights to model the discharge without that extra information. This has been found to prevent weights 'fixing' the erroneous outputs of other weights, preventing co-adaptation of weights and, ultimately, encouraging the model to use a simpler and more robust representation of rainfall-runoff processes (Srivastava et al., 2014). The hidden size determines

the total number of parameters in the model. For the LSTM there are 23,361 trainable parameters, whereas the EA LSTM has 14,593 trainable parameters. These are trained on data from 669 catchments over 4018 timesteps (2,688,042 samples). Note that this is for a regional model and is independent of the number of catchments. Given that we train the LSTM on 669 catchments, we can interpret the LSTM as equivalent to using 35 parameters per catchment, with a median catchment area of 152 km^2. The EA LSTM has on the order of 22 parameters per catchment. We chose the hyper-parameters (dropout rate, hidden size - hs) based on analysis of the NSE performances, finding that the improvement of further model complexity (increased hidden size) was negligible after a hidden size of 64. The hidden size was also consistent with the choices made in previous studies (Kratzert et al., 2019). We used the Adam optimisation algorithm (Kingma and Ba, 2014) and stopped training after 30 epochs, after which there was no further improvement to the model. An epoch reflects a single pass of the training dataset through the model, such that every sample in the training dataset has been used to update the model weights. This reflects the fact that during the training of DL models, the data are often split into batches to allow large datasets to be read into memory. The LSTM ensemble took 10 hours to train. The EA LSTM ensemble took 96 hours to train. All models were trained on a machine with 188GB of RAM and a single NVIDIA V100 GPU.

2.4 Model Performance Comparisons

The LSTMs learn to represent hydrological processes directly from data. When the LSTMs perform well on hold-out test samples, a necessary (but not sufficient) conclusion is that the data contains useful information about the hydrological processes that translate inputs (precipitation) into outputs (discharge). The differences in model performance between the LSTMs and the benchmark hydrological models can be used to determine hydrological processes that are described by the input data, but not captured or under-represented by the benchmark hydrological models.

2.4.1 Benchmark Models

In order to provide a reference for model performance statistics, we compare the performance of the LSTM based models against four lumped conceptual models from the FUSE framework (Clark et al., 2008). To be unbiased on the model calibration, we used simulated discharge time series from Lane et al. (2019) who calibrated and evaluated these four conceptual models on 1000 catchments across Great Britain. The four conceptual models used are: TOPMODEL (Beven and Kirkby, 1979), Variable Infiltration Capacity (VIC) (Liang, 1994), Precipitation-Runoff Modelling System (PRMS) (Leavesley et al., 1983) and SACRAMENTO (Burnash et al., 1973). These conceptual models are often used in operational settings, due to the relative ease of use and lower data requirements when compared with physically-based models. These conceptual models all explicitly maintain mass balance, and so assume no losses or gains of water other than flow from the catchment outlet or evaporation.

These conceptual models are all lumped models run at a daily time step. Each model is explicitly forced to close the water balance, limited by an upper limit of potential evapotranspiration for water losses. Every one of the conceptual models has a gamma distribution routing function. Furthermore, the four conceptual models do not include a snow routine nor a vegetation module (Clark et al., 2008). Sacramento has 5 stores and 12 parameters per catchment; VIC and TOPMODEL have 2 stores,

both have 10 parameters; PRMS has 3 stores and 11 parameters. A more complete description of these benchmark models and the processes that they include can be found in Table 3 of Lane et al. (2019) and in Section 4 of (Clark et al., 2008).

The benchmark study provides an assessment of conceptual model simulation performances across a large sample of GB catchments, and also quantifies uncertainty in hydrological simulations due to parameter uncertainty and model structural uncertainty (Lane et al., 2019). Parameter values for each conceptual model were selected from 10,000 simulations of multi-dimensional parameter space. The best-estimate model parameter values were selected from these 10,000 samples using the Nash-Sutcliffe Efficiency score. These best-fit parameters are used as a benchmark against which to compare the LSTM performance. To place the intercomparison in context, we critically reflect on the consistencies and differences between the different model configurations here.

First, the selection of model parameters differs between the LSTM and the conceptual models. The experimental design of the benchmarking study produced 10,000 samples of parameter values and Lane et al. (2019) provide the simulations given the best fitting parameters for future studies to employ as a benchmark. The LSTM parameters are optimised using stochastic gradient descent, choosing the best fitting set of parameters using the NSE score. While the method of choosing parameters differs, the objective function that determines the "best-fit" parameter values are the same for both the LSTMs and the conceptual models. Second, the calibration and evaluation data are the same. The calibration and evaluation of these models was performed using the same data from CAMELS-GB, i.e. the National River Flow Archive data (Centre for Ecology and Hydrology, 2016) for specific discharge (y_t), the Centre for Ecology and Hydrology Gridded Estimates of Areal Rainfall, CEH-GEAR, for precipitation (Tanguy, 2014) and the Climate Hydrology and Ecology research Support System Potential Evapotranspiration (CHESS-PE) data set for PET (Robinson et al., 2017). The benchmark experiment selected the best-fitting parameter values using data from the period 1988–2008, and then evaluated their performance on data from 1993–2008 (Lane et al., 2019). Instead, we calibrate the LSTMs on data from 1988–1998 and then evaluate the LSTM performances for our hold-out evaluation period of 1998–2008. We recalculate the performance statistics of the benchmark conceptual models for this evaluation period, 1998–2008, using the published simulated time-series. Therefore, the LSTM is evaluated on out-of-sample (in time) data, whereas, the conceptual model parameters were calibrated on data included in the evaluation period (in-sample evaluation). Finally, it is worth noting that Lane et al. (2019) focused not only on model performances but also on parameter uncertainty. Uncertainty is an essential component of any modelling study, and our approach of training an ensemble of 8 models is one proposed method for dealing with uncertainty in LSTMs. For an analysis of model uncertainty with this method see Appendix D. For a more complete treatment and discussion of the different approaches for dealing with uncertainty using LSTMs see Klotz et al. (2020).

As with any benchmarking study, there are important caveats to the intercomparison of model results. Ultimately, the purpose of the comparison is: (i) to provide a reference for the diagnostic measures of LSTM performance, (ii) to identify the hydrological conditions where simulations differ, and (iii) use these insights to diagnose missing representations in the conceptual models. We agree with Lane et al. (2019) that "benchmark [studies] provides a useful baseline for assessing more complex modelling strategies" (p.4029), and we follow them in publishing the simulations and results of the LSTM models for future studies to use for comparison.

2.4.2 Evaluation Metrics

Each model produces a daily simulated discharge value at each station. Three example hydrographs are shown in Appendix C. The evaluation metrics described below evaluate the overall performance of each model to reproduce a specific aspect of the observed hydrograph. For the LSTM-based models the evaluation metrics are calculated given the average discharge of the ensemble. Since no single evaluation metric can fully capture the performance of streamflow simulations across all flow-regimes (Gupta et al., 1998), we use a number of metrics to address the performance of models across the flow regime, outlined below.

We evaluate the goodness-of-fit of the LSTM based models and the conceptual models using six evaluation metrics. The Nash-Sutcliffe Efficiency (NSE) (Nash and Sutcliffe, 1970) score has been used in numerous studies and there is extensive literature discussing its strengths and weaknesses (Gupta et al., 2009). The NSE can be decomposed into three components, a correlation term, a bias term (BiasError) and a variability (SDError) term (Gupta et al., 2009). The bias term measures the error in predicting the mean flow. The variability term measures the error in predicting the standard deviation of discharge. We report results for the NSE and each of its three components.

To understand how well the LSTMs represent low, mean and high flows, we also consider the biases for different components of the flow duration curve. The low flow bias (%BiasFLV) is the diagnostic signature measure for long term base flow (Yilmaz et al., 2008), and low flows are defined as those which are exceeded 70% of the time. For the middle of the flow duration curve we use the bias of the mid section of the flow duration curve, between the 20th and 70th percentiles (%BiasFMS). Finally, we also look at the bias of the high flows, considering the top 2% of flows (%BiasFHV).

3 Results

3.1 National Scale Model Performance

The LSTM and EA LSTM models produce accurate simulations across Great Britain when evaluated using a variety of metrics, with differing levels of performance improvement over the benchmark conceptual models (See Table 3).

Comparing the median NSE for all catchments, the LSTM ensemble (0.88) outperforms all other models, including the EA-LSTM ensemble (0.86). The slightly lower median NSE for the EA-LSTM models is consistent with results from previous studies (Kratzert et al., 2019). The CDFs (cumulative distribution functions) of the NSE (Fig. 1a) show the entire distribution of LSTM scores is shifted towards better performances. The LSTM NSE scores are significantly different from all comparison models at $\alpha = 0.001$ (Paired Wilcoxon signed-rank-test). We see the same pattern for the EA-LSTM models. The performance improvement at the tails is particularly pronounced. Neither the LSTM nor the EA-LSTM model have any station gauges with an NSE of less than zero.

As discussed in the methods, we can decompose the NSE into three components, bias (BiasError), correlation and error in predicting the variability of flows (SDError). The pattern of correlation scores closely follows the pattern of NSE, with the entire distribution of catchment correlation scores shifted towards improved performance. The CDFs in Fig. 1c show that the

Table 3. Summary of all goodness-of-fit metrics used to benchmark performance against the conceptual models for the validation period 1998–2008 on the 518 stations found in both CAMELS-GB data (Coxon et al., 2020a) and the FUSE conceptual models (Lane et al., 2019). We have shown the median catchment score for the metric given the mean simulated discharge of our ensemble. Values that are not significantly different from the best model are highlighted in bold ($\alpha = 0.001$).

	NSE	BiasError	SDError	Correlation	%BiasFMS	%BiasFLV	%BiasFHV
TOPMODEL	0.76	-0.04	-0.10	0.88	**5.70**	42.22	-13.04
ARNOVIC	0.78	0.06	-0.10	0.90	**2.25**	-60.34	-14.66
PRMS	0.77	0.03	**-0.03**	0.89	35.24	-315.25	-15.11
SACRAMENTO	0.80	**-0.01**	-0.07	0.90	27.91	-195.92	-16.19
EALSTM	0.86	**-0.02**	-0.10	0.94	-6.29	**23.61**	-10.81
LSTM	**0.88**	**-0.02**	-0.09	**0.94**	-3.67	**26.34**	**-9.09**

LSTM catchment bias scores are closer to zero than the benchmark models, which reflects the fact that the conceptual models are explicitly mass-conserving, whereas the LSTM models are not. The median variability error is negative (Fig. 1d), showing that the LSTMs tend towards underpredicting the variability of flows.

The LSTM shows a large performance improvement for low-flow bias score (%BiasFLV - Fig. 1e). The LSTM has lower median bias in the slope of the midsection of the flow duration curve (%BiasFMS) than all models except ARNOVIC. When we consider the CDFs, both LSTMs have shorter tails than the conceptual models, showing that a greater proportion of catchments have biases closer to zero. The high-flow biases (%BiasFHV) are relatively similar for all models, as shown by Fig. 1g).

The biases at different flow exceedances suggest that the conceptual models produce good simulations for the high flows, but are less able to simulate low flows. The LSTM shows a smaller performance decline at the low flows than the benchmark models and a competitive performance at high flows, suggesting that the LSTMs are robust to extreme conditions. We also note that the negative bias, for the midsection and the upper-section of the flow duration curve, demonstrates that the LSTM model is conservative in its flow predictions, particularly in comparison to the other models.

3.2 Spatial Patterns of Performance

The LSTM demonstrates competitive simulation of discharge across Great Britain (see the spatial patterns of various performance metrics in Appendix Fig. E1). The EA LSTM has very similar spatial patterns to the LSTM, but shows a consistently worse performance than the LSTM across GB.

The benchmark conceptual models struggled when simulating discharge in catchments on the permeable bedrock in the South East of England and the mountainous catchments in the North East of Scotland (Lane et al., 2019). Performance metrics in the South East were lower due to poor simulation of variance and correlation, and in North-Eastern Scotland due to poor simulation of the mean flow conditions (Lane et al., 2019). We suggest that these differences in performance are due to the
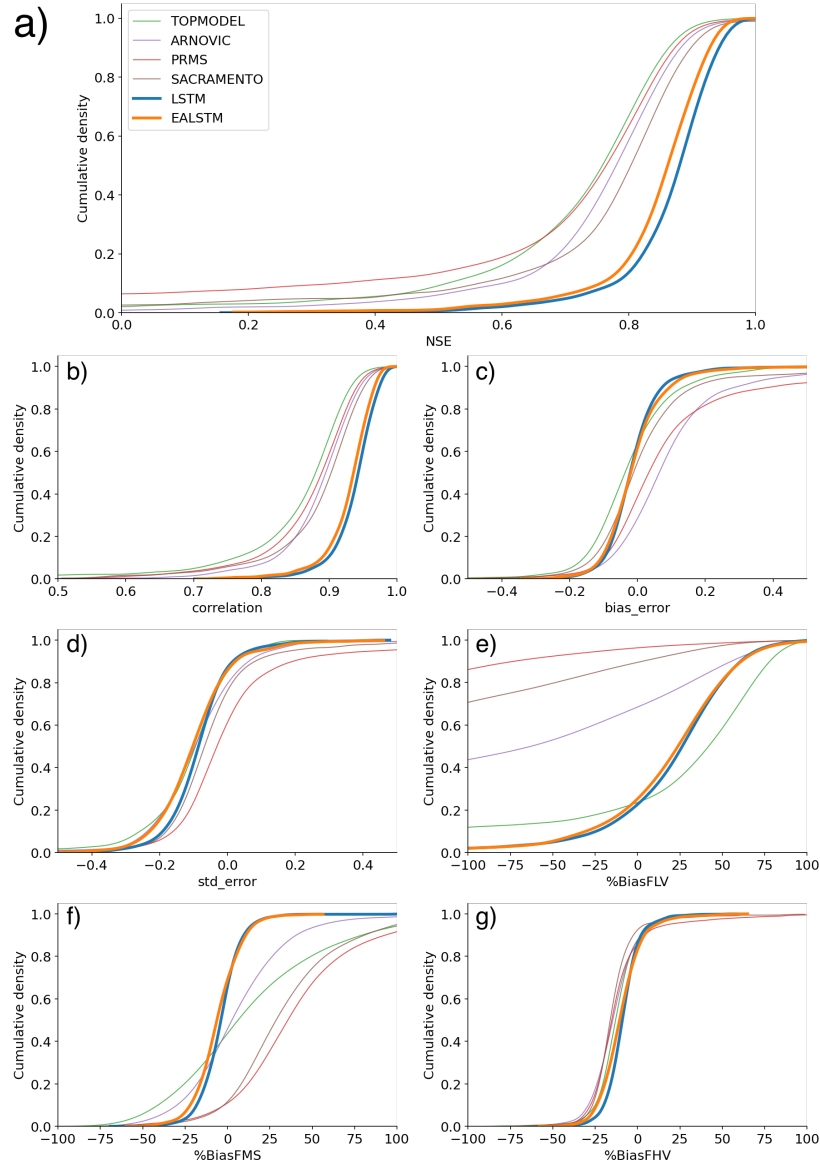
Figure 1. Cumulative Distribution Functions (CDFs) of station goodness-of-fit metrics scores for each model. EALSTM (orange) and the LSTM (blue), and the conceptual models: TOPMODEL (green), VIC (red), PRMS (purple), Sacramento (brown) (Lane et al., 2019). Panels indicate distribution of station: a) NSE scores b) correlation scores c) bias error scores d) variability error scores e) low-flow bias scores f) mid-range of flow bias scores g) high-flow bias scores

low rainfall and chalk aquifer in the South East of England, and to the lack of snow modules incorporated into the conceptual models for North East Scotland.

Interestingly, the LSTM simulates discharge less well in the South East of England relative to LSTM performance elsewhere in GB, particularly in the summer months (Fig. 2). Performances for all seasons are worse in the South East of England. This pattern is stronger in the summer months (JJA). The East-West gradient in model performances can be seen for all models, particularly in JJA. However, the range of errors is smaller for the LSTM based models when compared with the conceptual models.

The LSTM shows an underestimate of the variability and a cluster of high bias scores in the South East (Appendix Fig. E1). The LSTM both overestimated and underestimated mean flows in catchments in the South East region, explaining the relative under-performance in the composite metric (NSE) for the LSTM relative to the rest of GB.

Spatial patterns in the biases for different sections of the flow duration curve show that only the LSTMs demonstrate a consistent underprediction of the midsection slope of the flow duration curve (%BiasFMS). A steep slope in the midsection of the flow duration curve reflects a watershed having a "flashy" response (Yilmaz et al., 2008), potentially due to low soil moisture capacity. Therefore, an underprediction of the midsection reflects an underestimation of the "flashiness" of the catchment. The LSTM %BiasFMS is largest for the South East of England. The LSTM shows improved performance compared to the benchmark models across GB, including these under performing regions, the South East of England, and North East Scotland.

3.3 In what hydrological conditions do model performances differ?

Large sample studies allow us to detect catchment attributes that our models are (not) able to represent. In order to determine what the LSTM is capable of representing well we perform two analyses. Firstly, directly calculating the difference in NSE scores. Secondly, we correlate catchment attributes with model diagnostic scores.

The Δ_{mean}NSE is the mean difference between a reference model (LSTM) and the comparison model. The Δ_{median}NSE is the median difference. The mean differences between the LSTM station NSE and the other models is smallest for the EA-LSTM (Δ_{mean}NSE = 0.02). This is unsurprising given the very similar architectures of the two models. The differences for the conceptual models range from TOPMODEL (Δ_{mean}NSE = 0.15); ARNOVIC (Δ_{mean}NSE = 0.17); SACRAMENTO (Δ_{mean}NSE = 0.20), and PRMS (Δ_{mean}NSE = 0.43). While the mean performances show large differences, due to the presence of poorly performing stations, the median differences are smaller SACRAMENTO (Δ_{median}NSE = 0.07); ARNOVIC (Δ_{median}NSE = 0.09); PRMS (Δ_{median}NSE = 0.10) and TOPMODEL (Δ_{median}NSE = 0.10). Both summaries (median, mean) demonstrate that the LSTM offers a single model architecture that offers more accurate simulations than traditional hydrological models in a variety of hydrological conditions.

Spatially, the benchmark conceptual models struggled to produce good simulations in two geographical regions. These were in the South East of England and North East of Scotland. The performance improvement (ΔNSE) of the LSTM over the conceptual model was indeed largest in the South East of England and North East Scotland (see Fig. 3).

North East Scotland is one of the most mountainous regions of GB. The Cairngorm National Park and the North Pennines are the only areas of GB where snow processes are consistently important, owing to catchments having a higher elevation. There are 36 catchments in the CAMELS GB dataset with fraction of snow cover greater than 5%, and three are in the North Pennines, the other 33 are in the Cairngorm National Park. The results in Fig. 3 show that the LSTM exhibits a large
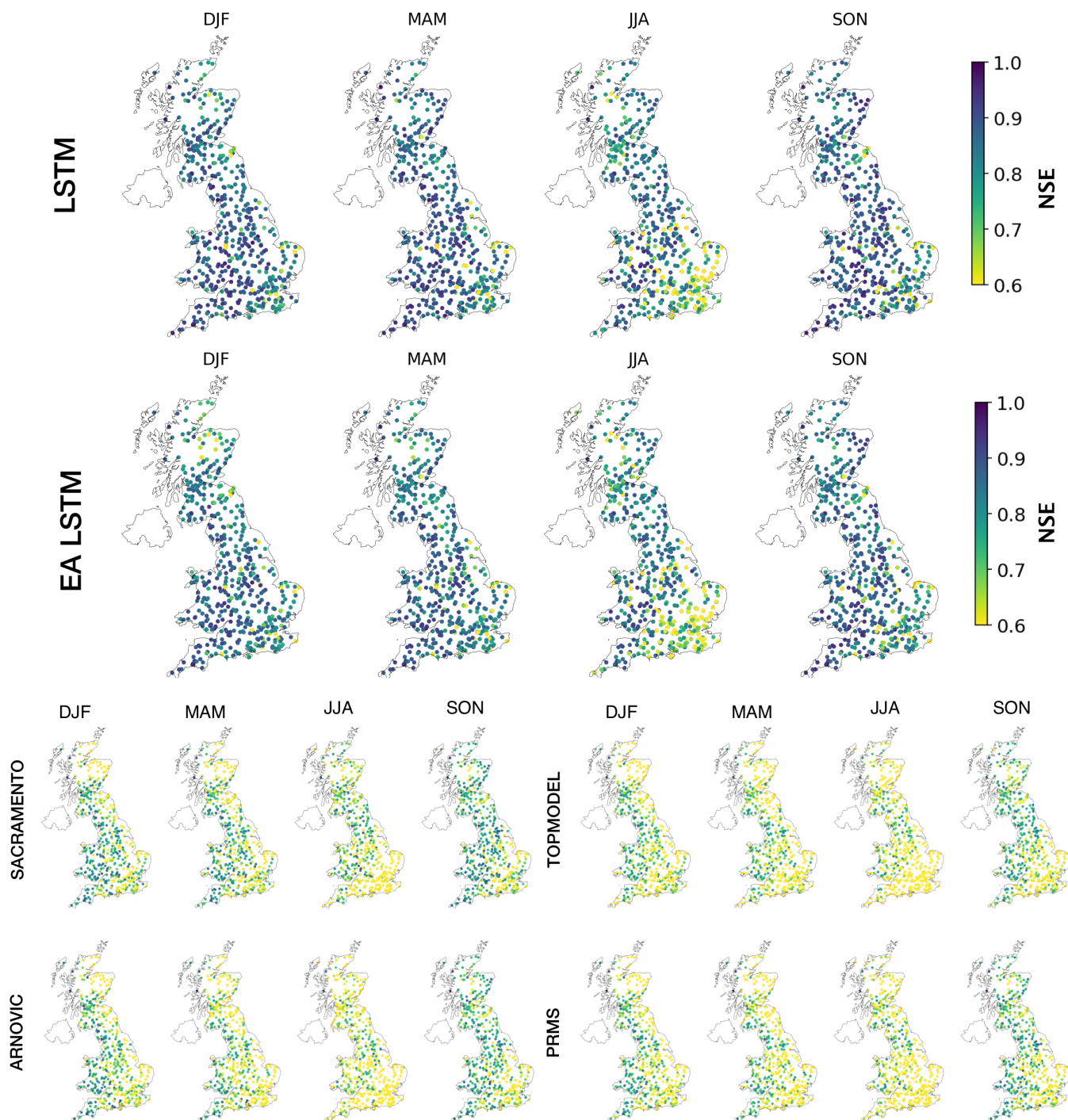
Figure 2. Seasonal NSE patterns for the two LSTM based models (above) and the conceptual models (below). Each station in the evaluation data is shown as a point. The colour of the point reflects the NSE score. Brighter colors reflect lower NSE values, currently capped at a minimum of 0.7 NSE.
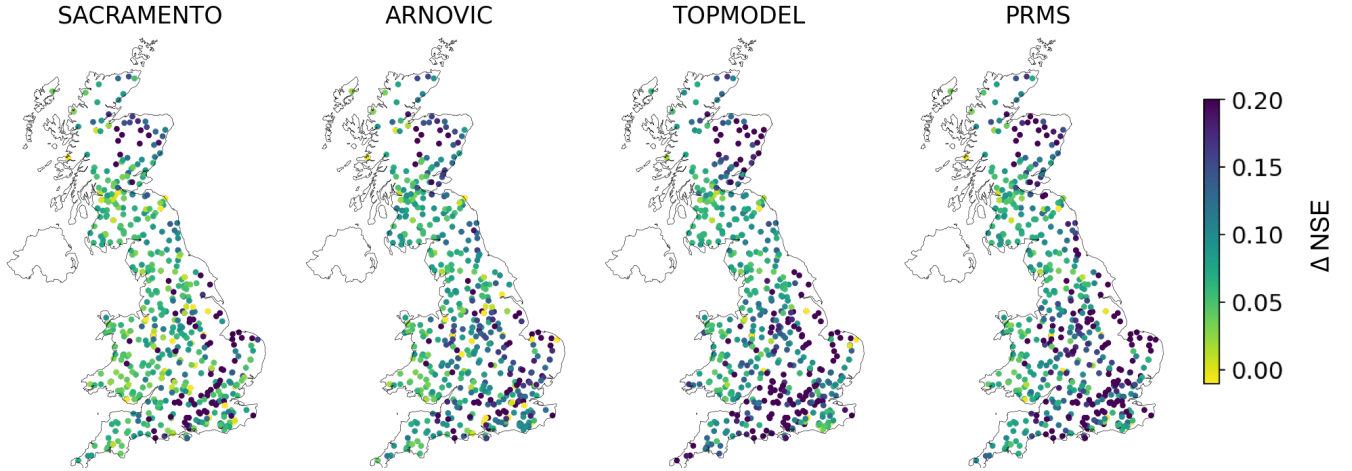
Figure 3. The performance improvement of the LSTM relative to the four conceptual models, SACRAMENTO, ARNOVIC, TOPMODEL and PRMS. The difference in NSE is calculated by subtracting the conceptual model NSE from the LSTM NSE ($\Delta NSE = NSE_{LSTM} - NSE_{conceptual}$). Each point represents a station and the colour reflects the performance improvement (measured by NSE) of the LSTM compared with the conceptual models. Positive values reflect stations where the LSTM outperforms the conceptual models.

performance improvement in these catchments, since ΔNSE is high. This is most likely due to the cell state being able to
325 represent longer-term stores and fluxes of water, therefore capturing the melting snow processes. The conceptual models lack a snow module, and are therefore unable to capture snow melt or frozen ground processes, which are especially important in winter (DJF) and spring (MAM) (Lane et al., 2019). By contrast, what the LSTM performance shows is that data-driven models are able to flexibly incorporate snow processes in the catchments where they are required (NE Scotland) even when trained to produce one set of weights. This flexibility is an important asset of data-driven approaches, since these hydrological processes
330 do not need to be specified prior to model training, but can be learned from the available data.

The South East is a relatively dry area, with large chalk aquifers contributing to a high baseflow index and large urban and agricultural areas, contributing to a large anthropogenic signal in the hydrographs. Although the improvement in simulation accuracy compared to the conceptual models is large in the South East, the pattern of raw LSTM NSE shows that the LSTM still underperforms in the South East relative to elsewhere in GB. The seasonal patterns showed that the LSTMs performed
335 worse in summer months, which is the drier period of the year. Consistent with this spatial pattern, the ratio of mean potential evapotranspiration to mean precipitation attribute (labelled "*aridity*" in the CAMELS GB dataset (Coxon et al., 2020b)) is negatively correlated with model performance for all models (Fig. 4), although the magnitude of this association is smaller for the LSTM based models than the conceptual models.

We observe consistently poorer performance across all models, including the LSTMs, in drier hydrological conditions. This
340 can be seen by the negative correlations between catchment P/PET (aridity) and model NSE scores (Figure 4).
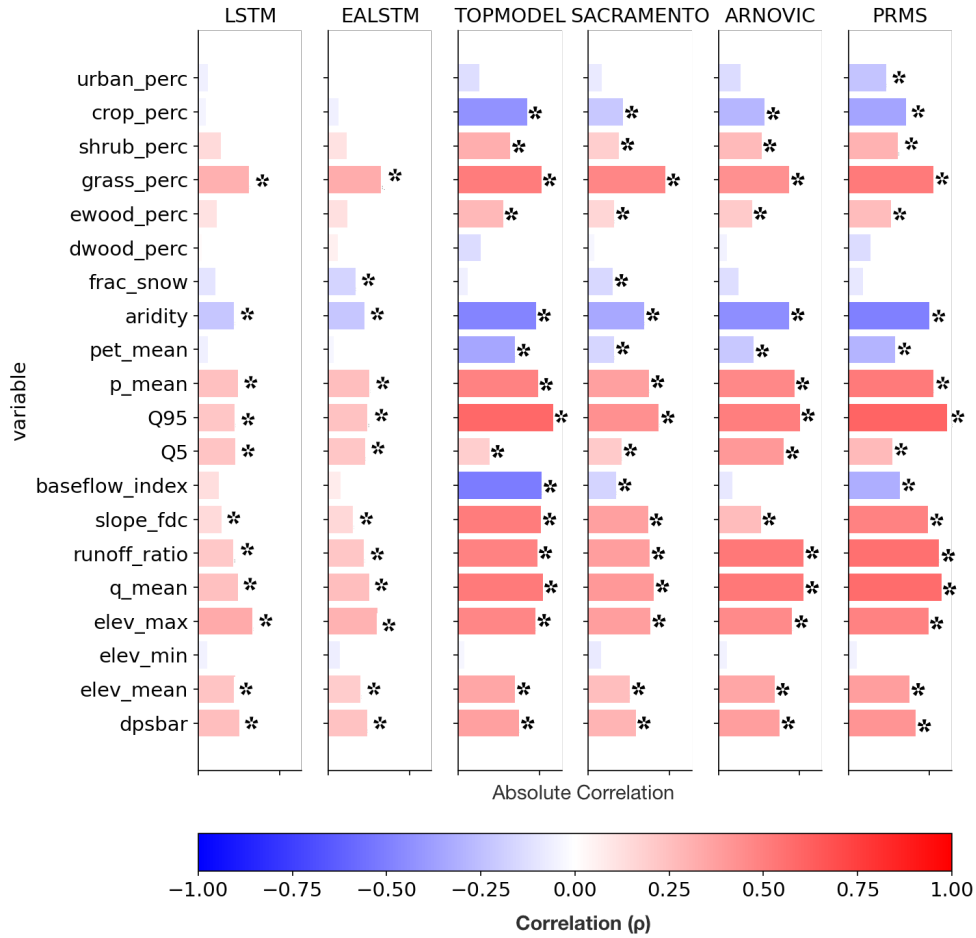
Figure 4. Static features (rows) and their Spearman's Rank Correlation Coefficient with model (columns) NSE scores. The positive correlations are in blue, the negative correlations are in red. Pale bars show very low correlations. (*) indicates that the correlation is significant at the α=0.001 level. The first 6 features can be classified as landcover features. The next 4 features are climatic indices. The next 6 features are hydrologic attributes and the final 4 are topographic features. DPSBar refers to the mean drainage path slope, and reflects the average steepness of a catchment.

The LSTM-based models show no significant correlation between baseflow index and model performances, in contrast with the other models. ARNOVIC also shows no significant correlation. ARNOVICs improved performance can be attributed to the non-linear relationship in the upper-storage, which means that the model will only produce very fast responses when that storage is very close to full (Lane et al., 2019).

3.3.1 The impact of water balance closure on simulation accuracy

One of the key hydrological conditions that hydrological models struggle with is the lack of closure of the catchment water balance. The conceptual models we test here explicitly maintain mass balance. They define the topographic surface water catchment as the surface over which water is conserved, i.e. the surface water catchment is not expected to leak, nor should any water enter the catchment other than through measured precipitation. This will not then capture water losses or gains from undercatch, drifting snow, advection of fog, groundwater, or anthropogenic transfers into or out of the topographic catchment. Consequently, we would not expect the conceptual models to take account of catchments where the water balance (defined in the data) does not close. The LSTM, in contrast, is free to adjust to account for patterns in these anomalies. It is not yet possible to diagnose the origin of any such anomalies using the LSTM alone: they may arise from inter-catchment transfers (either through anthropogenic or groundwater processes), or data errors, among other reasons that the water balance might not be closed based on observations at the catchment scale. In spite of this, we expect that the LSTM will show improved performance in these catchments where there is no closure of the catchment water balance in the underlying dataset. Since we are calculating performance on out-of-sample timesteps, if the LSTM performance is improved, we can infer that the LSTM based model has learned to correct these inconsistencies in a way which is consistent between training and evaluation data, and is therefore adjusting the catchment water balance to better simulate the hydrograph.

We plot catchments on two dimensions (Fig. 5), their wetness index (P/PE) and the runoff coefficient (Q/P), to identify catchments where water is not conserved. Points above the horizontal line reflect catchments where the observed discharge is greater than the precipitation input to the catchment. This area of the graph represents catchments where the data has too little water to generate the observed runoff. Points below the curved line are where runoff deficits exceed total PET in a catchment. This area of the graph represents catchments where PET is not large enough to describe the water remaining after runoff is accounted for, i.e. the data has "excess" water (Fig. 5).

We tested whether the LSTM was better able to simulate discharge in catchments with "excess" water (i.e. the points below the curved lines in Fig. 5, which are then represented by the orange kernel density estimate in Fig. 6). As hypothesised, we find that the LSTM is more robust to these conditions and produces NSE scores that are comparable to the stations where the conceptual models perform best.

Interestingly, despite the performance improvement over the benchmark conceptual models the LSTMs continue to produce a performance decline in catchments with an imbalanced water balance (Fig. 6). This suggests that the LSTM models still struggle with water-limited and energy limited (low runoff coefficient and low wetness index) catchments. This could be because human management decisions that lead to abstractions are unpredictable without further dynamic inputs, such as timings of abstractions and effluent returns. Or else, that the underlying data does not contain sufficient geological information to describe the complex percolation and surface or subsurface connectivity pathways that cause a surface water catchment to leak.
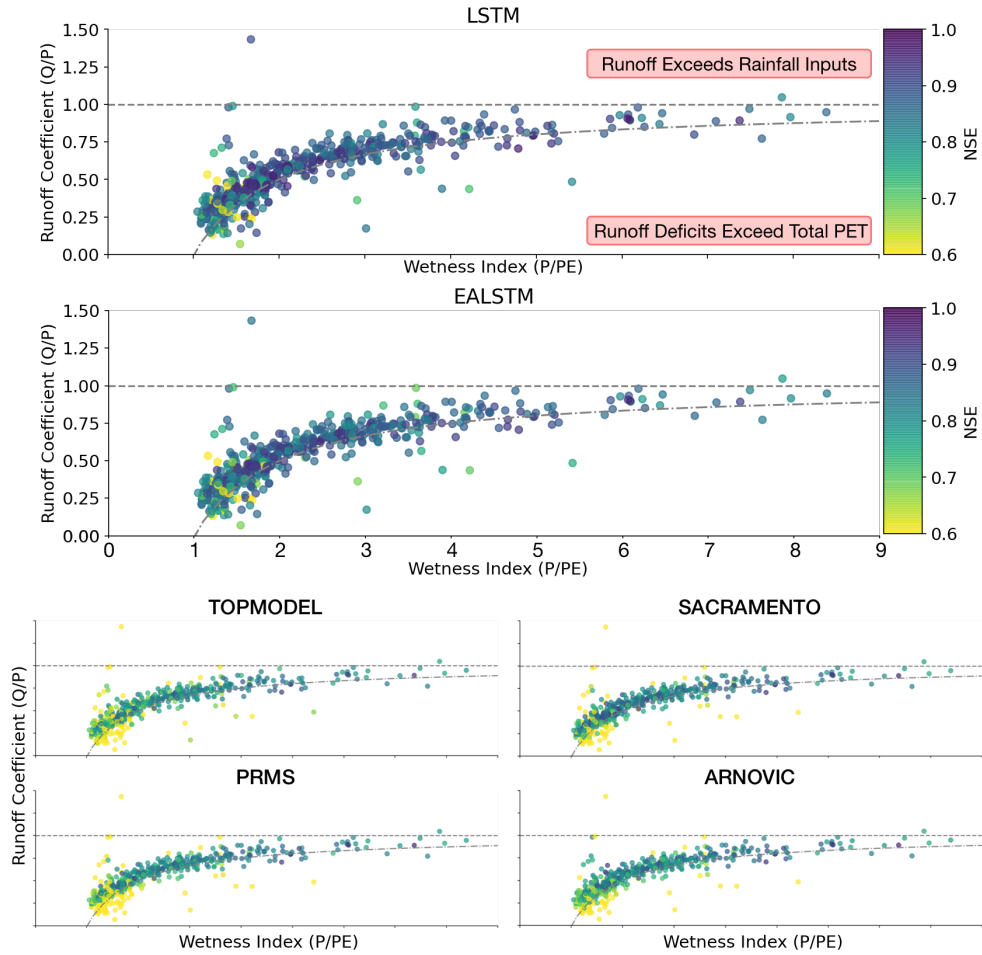
Figure 5. Scatter plot for the relationship between the wetness index, runoff coefficient and the model NSE score. Each point is a catchment, coloured by the NSE score ranging from 0.8 (lighter) to 1.0 (darker). Points above the horizontal line reflect catchments where the observed discharge is greater than the precipitation input to the catchment. Points below the curved line are where runoff deficits exceed total PET in a catchment, therefore, there is "excess water" in the data, since PET cannot explain the leftover water after accounting for runoff.

Ultimately, the performance decline is less pronounced for the LSTM. The LSTM continues to produce simulations with NSE scores greater than 0.6. This suggests there remains information in the data that the LSTM is capable of using to maintain accurate simulations in out-of-sample conditions.

4 Discussion

This study benchmarks the performance of the LSTM using four commonly-used conceptual models as a reference. The LSTM produced accurate simulations for a large number of catchments across Great Britain. The performance of the LSTM

380
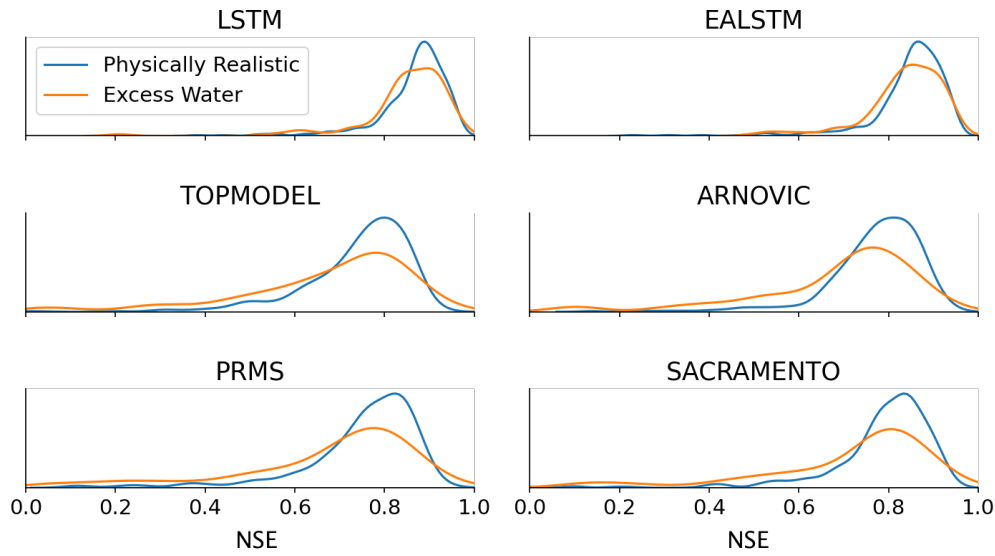
Figure 6. Comparing the NSE results for catchments that have excess water, where runoff deficits exceed total PET (orange) to those catchments that have physically realistic conditions (blue). The orange line shows the histograms for stations that fall below the curved line in the Budyko analysis above (the runoff deficit exceeds total PET, therefore there is excess water in the model). The blue line shows the histograms for those stations between the two dashed lines.

demonstrates that there is adequate information in the observational data to accurately simulate discharge behaviours across the various hydrological conditions found in Great Britain. The simulated time series and catchment error metrics can be found at: zenodo.org/record/4555820.

In the discussion that follows we return to our three research questions: (i) How well do LSTM-based models simulate discharge in Great Britain? (ii) How do LSTM-based model performances compare with the conceptual models used as a benchmark? (iii) Can we extract information from the spatial and temporal patterns in diagnostic measures?

4.1 Inter-Model Performances

The LSTM based models produce accurate simulations of discharge across GB, a temperate region. Two findings from this research confirm and extend the conclusions of previous work. First, the LSTM consistently outperforms the EA-LSTM (Kratzert et al., 2019). Secondly, both LSTM-based models demonstrate improved simulation accuracy for discharge modelling compared with the conceptual models we use as benchmarks.

4.1.1 How well do LSTM-based models simulate discharge in Great Britain?

The EA LSTM is constrained to treat information that does not vary over time (catchment attributes) separately from information that varies over time (hydro-meteorological forcings). However, the constraint penalizes performance, which was also found by Kratzert et al. (2019). The EA LSTM, in contrast, is forced to keep the input gate static through time. The input gate

receives only information about catchment attributes. This means that no time-varying information is passed through the EA LSTM input gate. In contrast, the LSTM gates receive information from both time-varying meteorological inputs and static catchment attributes. The under performance of the EA LSTM relative to the LSTM suggests that this regularisation hurts performance in out-of-sample conditions.

It is worth noting that the LSTM and EA-LSTM also differ in terms of practical computational requirements. The LSTM trains much faster than the EA-LSTM. The LSTM will train 30 epochs in 1 hour, compared with 30 epochs in 10 hours for the EA-LSTM. This is due to the LSTM being an in-built Pytorch (v.1.7.1) function that makes use of CUDA optimised code (for running the models on a GPU). In contrast, the EA-LSTM relies on custom code without the CUDA enabled optimisations.

4.1.2 How does the LSTM performance compare with the conceptual models used as benchmark?

We have demonstrated that the LSTM is an effective model architecture for extracting information from hydro-meteorological data, providing a data-driven benchmark showing what is achievable given the information contained in available observation data from CAMELS-GB (Nearing et al., 2020a). The LSTMs demonstrate better performance on out-of-sample times than in-sample performance from the benchmark conceptual models.

There are obvious challenges with direct comparison of LSTM performance against the benchmark developed by Lane et al. (2019). The first is that the LSTM is not constrained to maintain water mass balance, whereas the conceptual models discussed here are. Another challenge is that the method of optimisation used for choosing parameters in the LSTM (stochastic gradient descent) is different to the random-sampling and NSE selection criteria used to select the "best" model parameters for the conceptual models. The sampling process used by Lane et al. (2019) is explicitly for estimating uncertainty as well as providing a reference of conceptual model performances. Another difference is that the LSTM diagnostic scores are calculated on out-of-sample predictions, compared with the in-sample predictions for the benchmark conceptual models.

Finally, the LSTM-based models are trained on all basins, with a single set of weights for the whole of GB. Therefore, these LSTM models are regional models that are able to reproduce behaviours across Great Britain. In contrast, most hydrological models perform best when calibrated on individual basins (Beven, 2006a). By contrast, LSTM-based models are most accurate when trained with as much data from as many catchments as possible (Gauch et al., 2021b). It is important to interpret the number of parameters for each model type in light of this fact.

The catchments where the comparative performance difference is small, i.e. where the conceptual models perform almost as well as the LSTM, reflect areas where the conceptual models capture the majority of the information from the data, and the conceptual model well represents the hydrological process. This is the case in West Scotland, North West England & North Wales and North East England (see Appendix Fig. E2). The benchmark results are valuable in providing a reference point for us to assess the value of LSTM-based approaches. We welcome future studies using the LSTM simulations provided here and further explore performance differences and the limitations of DL methods across GB.

4.1.3 Can we extract information from the spatial and temporal patterns in diagnostic measures?

430 The LSTM shows the largest performance improvement over the conceptual models in the North West of Scotland and the South East of England. The performance differences in North West Scotland are very likely a result of the ability of the LSTM to learn a representation of snow processes from the input data, whereas, the conceptual models were simulating these catchments without a snow module.

Despite the performance improvement over conceptual models in the South East of England, the LSTM still struggles in
435 the South East relative to elsewhere in GB. The South East is a relatively dry region compared to elsewhere in GB. It contains the highest proportion of catchments that fall below the dashed line in Fig. 5, and therefore stations where the surface water catchment is "leaky". Furthermore, there are underlying chalk aquifers which provide water storage and lateral transfers. We outline three hypotheses for why the LSTM performance may be lower in the South East compared with elsewhere in GB.

The first hypothesis is linked to the training of the LSTM based models. The LSTM shows a performance decline in drier
440 conditions (Fig. 4, see "*aridity*"). This confirms the findings of other DL studies in the US, where the LSTM also struggled to reproduce hydrographs in drier conditions (Kratzert et al., 2019, 2018). Basins that have long periods of low flow contain little information, since changing meteorological inputs co-occurs with very little change in the target discharge. Therefore, the physical process relating meteorological inputs to river discharge can only be inferred from those catchments with varying discharge. There is some evidence for this hypothesis. NSE scores show positive correlations with increased discharge (at mean
445 flow, Q5 and Q95), as well as increased NSE as rainfall increases (p_mean) (Fig. 4).

A related, but separate, hypothesis is that the use of NSE as an objective function fails to adequately weight performance in these low flow regimes (the NSE was the objective function across both the conceptual models and the DL models).

A final hypothesis is that groundwater dynamics and human abstractions, which influence catchments in the South East, are not well captured by the variables in CAMELS-GB. Hydrological processes are not simulated as effectively in "leaky"
450 catchments compared to those catchments where the water balance can be closed with hydrometric data (Section 3.3.1), even using a very flexible and effective data-driven model that is not constrained to balance water (the LSTM). This suggests that the underlying data does not contain sufficient information to model the full range of processes that influence the hydrograph in these catchments, including groundwater and abstractions. The catchment averaged information on soil texture (sand-silt-clay) provides a coarse proxy for catchment porosity. Furthermore, further data, such as groundwater time-series, might be necessary
455 to obtain more accurate discharge predictions. We suggest that different input data sets should be tested to try and improve LSTM performances enabling the LSTM to more properly account for the complex percolation and infiltration dynamics in these catchments.

In terms of the seasonal patterns in LSTM performances and the worse performances in summer, the above hypotheses also apply, since the summer is the driest season in GB. Despite this, the LSTM-based models have been able to use the
460 information in the available data to better model summer (JJA) discharge than the benchmark models. As in the data-based mechanistic modelling framework (Young, 2003) the next stage for hydrologists is to search for a mechanistic interpretation of the learned model structure, also see Nearing et al. (2020a). One possible mechanistic interpretation that warrants further

exploration is the idea that the LSTM is capable of learning seasonally varying catchment "connectivity" (Bracken and Croke, 2007). In winter, when soils are saturated, there are a greater number of pathways for water to enter river channels, and

465 connectivity is high. In summer, however, there is greater resistance to water flow, since water can be absorbed and stored in drier soils, as found in Swiss catchments by van Meerveld et al. (2019), and connectivity is lower. Connectivity information could be represented by the hidden state ($\mathbf{h_t}$), or cell state vectors ($\mathbf{C_t}$). The proposed impact of catchment connectivity on the performance improvement of the LSTM based models is ultimately speculative, and future work will explore whether the LSTM has learned to represent the concept of connectivity and seasonally variable flow pathways.

470   In contrast with the benchmark conceptual models, the LSTM-based model NSE scores have no negative correlation with crop cover percentage (Fig. 4). It is possible that the LSTM has effectively used the cropland cover variable to improve its internal representation of hydrology in those catchments with a strong agricultural signal. In order to test this hypothesis, one could perform an ablation study, removing input features and determining the impact on model performances. Alternatively, sensitivity analysis could be used to determine the relative contribution of the input features to the discharge prediction, thus

475 revealing what input features are important for the model simulations. We intend to pursue this idea in upcoming papers.

     Ultimately, compared with the benchmark models, the LSTM shows robustness to catchment conditions associated with poor conceptual model performance. Dry catchments, catchments with a strong agricultural signal, and summer discharges are all strongly correlated with worse conceptual model performances. In contrast, the LSTM has good performance on out-of-sample times in these same conditions. There is therefore information that the LSTM has learned to generalise from the CAMELS-GB

480 dataset that the conceptual models are not utilising. The experiments we present here demonstrate conditions in which we can (and cannot) improve our traditional hydrological models given the availability of high quality, large sample datasets (Nearing et al., 2020c; Beven, 2006b).

5   Conclusions

In this study we have benchmarked the performance of two LSTM based models trained on 669 catchments across Great

485 Britain. We have demonstrated that LSTM-based models trained on a large sample of catchment-averaged hydro-meteorological time-series produce accurate simulations across GB. There is clearly information available in CAMELS-GB for modelling diverse hydrological conditions, and the LSTM performances should be interpreted as a competitive reference for what simulation performance is possible on out-of-sample (in time) conditions. We trained an ensemble of LSTM-based models to account for random initialisation during the training process of these deep learning models, which also provides an estimate of predic-

490 tion uncertainty (Appendix D). The ensemble mean simulation produces a median NSE score of 0.88 (LSTM) and 0.86 (EA LSTM), with no catchments scoring NSE below 0. These results are consistent with the findings from Kratzert et al. (2018) in a different geographical context.

     We have explored the spatial and temporal patterns in LSTM and EA LSTM performances, using the large-sample of catchments to better understand the conditions in which the LSTM-based models perform well, compared to themselves (LSTM

495 in catchment A vs. LSTM in catchment B) and compared with traditional conceptual models. The results show that LSTM-

based model performances are more robust to hydro-climatic conditions in the South East of England, in more arid catchments and in catchments where the water balance does not close. This suggests that there is more information in large-sample datasets such as CAMELS-GB than is captured by hydrological theory as encoded in the benchmark conceptual models. Further work remains to determine what information has been learned by these LSTM-based models, to use that information to improve hydrological theories, and feed them back, if possible, into further developments in conceptual and physically based models.

Relative to the LSTM-based model performances elsewhere in GB, the LSTM-based models continue to underperform in South East England relative to elsewhere in GB. Considering the catchment conditions that are associated with this pattern it is clear that all models struggle with drier conditions and catchments where the water balance does not close. It also seems possible that the training process fails to capture hydrological behaviours in drier catchments. There are a number of possible reasons. Firstly, changing meteorological conditions in dry catchments lead to little or no change in discharge (as would be the case in ephemeral streams). Alternatively, the LSTM architecture may not be capable of simulating both dry catchments and those with a higher runoff-ratio using just a single set of weights. Finally, the data may not contain sufficient information to capture the percolation and connectivity dynamics that drive hydrological behaviour in catchments with significant groundwater processes. Further studies will examine the internal representation of hydrological processes in these catchments to better understand what the LSTM has (not) learned about connectivity and groundwater processes.

This paper benchmarks LSTM performance across Great Britain using a new large-sample dataset, CAMELS-GB (Coxon et al., 2020b), providing a reference for future hydrological modelling efforts. Furthermore, this manuscript outlines the hydrological conditions in which the LSTM-based models perform well and those conditions which are more difficult to model. We encourage future benchmarking studies to include LSTMs as a competitive model choice for simulating rainfall-runoff processes.

Code and data availability. CAMELS-GB data is available at: https://catalogue.ceh.ac.uk/documents/8344e4f3-d2ea-44f5-8afa-86d2987543a9. The FUSE benchmark model simulations are available at: https://data.bris.ac.uk/data/dataset/3ma509dlakcf720aw8x82aq4tm. The neuralhydrology package is available on github here: https://github.com/neuralhydrology/neuralhydrology. The model simulations are freely available here: zenodo.org/record/4555820. The predictions and error metrics for the fitted models can be found online here: zenodo.org/record/4555820

Appendix A: LSTM and EA LSTM Model Description

The LSTM captures information that is important over both long and short term time horizons, overcoming a key difficulty with traditional RNNs, which are unable to retain information over longer sequences (Hochreiter, 1991; Bengio et al., 1994). LSTMs do this by maintaining two state vectors, a cell memory vector that captures slowly evolving processes ($\mathbf{C_t}$, Eq. A5) and a more quickly evolving state vector, colloquially named the "hidden" vector ($\mathbf{h_t}$, Eq. A6). The $\mathbf{C_t}$ vector, accounts for longer-term dependencies, and a series of 'gates' control the information passing into and out of the memory vector. The $\mathbf{h_t}$ vector evolves more quickly depending on input information and the output of the memory vector (see Fig. A1). The gates include: the forget

gate ($\mathbf{f_t}$), which controls the elements of the cell memory vector that are forgotten (i.e. how long water persists in the system, Eq. A1); the input gate ($\mathbf{i_t}$), which controls what information from the new input data at that timestep will be incorporated into the cell memory vector (i.e. what information is stored for future timesteps, Eq. A2); and finally the output gate ($\mathbf{o_t}$), which

530   determines what information from the cell memory will be used to update the hidden state (i.e. what information will impact discharge at the current timestep, Eq. A3). These gates are neural network layers, made up of weights (W_{layer}), biases (b_{layer}) and activation functions. The activation functions allow the LSTM to model nonlinear processes. During training, we seek the values for these weights and biases that best describe observed discharge. The information that passes through the input gate to the cell state ($\mathbf{C_t}$ - see Eq. A5) is itself processed through a neural network layer, producing a series of candidate values

535   that may be used to update the cell state (Eq. A4). Finally, information from the cell state is passed through the output gate ($\mathbf{o_t}$) to produce the hidden output ($\mathbf{h_t}$) at that time-step (Eq. A6). Note that for the LSTM we have explicitly defined the inputs as the concatenation of the dynamic meteorological data and the static catchment attributes, $[\mathbf{X_{t,n}}, \mathbf{A_n}]$. That is, both LSTM models receive the same information. We refer the reader to Kratzert et al. (2018) and Kratzert et al. (2019) for comprehensive descriptions of the LSTM and EA LSTM, and their hydrological interpretation.

540
$$\mathbf{f_t} = \sigma \left(\mathbf{W}_{\text{f}} \left[\mathbf{X_{t,n}}, \mathbf{A_n}, h_{t-1} \right] + b_{\text{f}} \right) \tag{A1}$$

$$\mathbf{i_t} = \sigma \left(\mathbf{W}_{\text{i}} \left[\mathbf{X_{t,n}}, \mathbf{A_n}, h_{t-1} \right] + b_{\text{i}} \right) \tag{A2}$$

$$\mathbf{o_t} = \sigma \left(\mathbf{W}_{\text{o}} \left[\mathbf{X_{t,n}}, \mathbf{A_n}, h_{t-1} \right] + b_{\text{o}} \right) \tag{A3}$$

$$\tilde{\mathbf{C}}_{\mathbf{t}} = \tanh \left(\mathbf{W}_{\text{C}} \left[\mathbf{X_{t,n}}, \mathbf{A_n}, h_{t-1} \right] + b_{\text{C}} \right) \tag{A4}$$

$$\mathbf{C_t} = \mathbf{f_t} * C_{t-1} + i * \tilde{C}_t \tag{A5}$$

545
$$\mathbf{h_t} = \mathbf{o_t} * \tanh(\mathbf{C_t}) \tag{A6}$$

The EA LSTM was developed specifically for rainfall-runoff modelling (Kratzert et al., 2019). The key difference between the EA LSTM and the LSTM is that the input gate (i) is no longer conditional upon the dynamic (time-varying) data. Instead, the static (time-invariant) catchment attributes ($\mathbf{A_n}$) exclusively influence the input gate (Eq. A2 is replaced with Eq. A8), and all other gates are solely influenced by the dynamic input data (Eq. A7, A9, A10).

550
$$\mathbf{f_t} = \sigma \left(\mathbf{W}_{\text{f}} \left[X_t, h_{t-1} \right] + b_{\text{f}} \right) \tag{A7}$$

$$i = \sigma \left(\mathbf{W}_{\text{i}} A + b_{\text{i}} \right) \tag{A8}$$

$$\mathbf{o_t} = \sigma \left(\mathbf{W}_{\text{o}} \left[X_t, h_{t-1} \right] + b_{\text{o}} \right) \tag{A9}$$

$$\tilde{\mathbf{C}}_{\mathbf{t}} = \tanh \left(\mathbf{W}_{\text{C}} \left[X_t, h_{t-1} \right] + b_{\text{C}} \right) \tag{A10}$$

The EA LSTM is described as "entity-aware" because it explicitly learns how to use $\mathbf{A_n}$ to distinguish between similar

555   dynamic inputs ($\mathbf{X_{t,n}}$) for different catchments ("entities"). For the EA LSTM, i is determined solely by the catchment attributes (Eq. A8). Therefore, each catchment has one unique hs dimensional vector which controls what information should
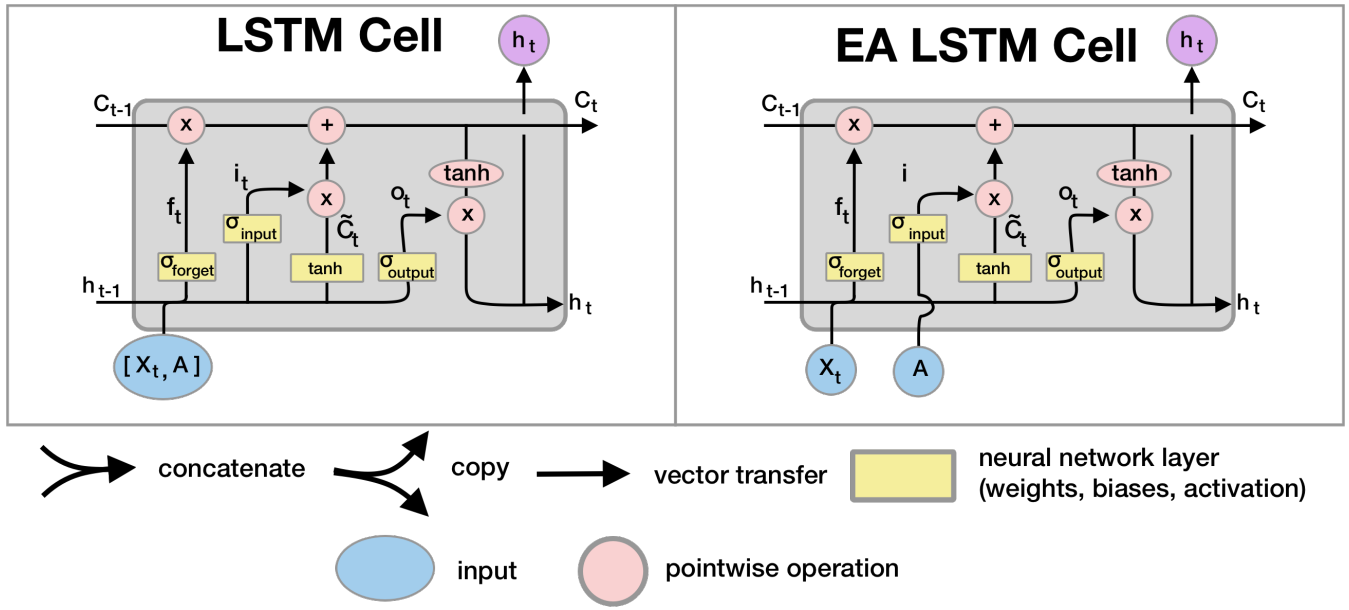
Figure A1. Wiring diagram for the LSTM and EA LSTM recurrent cells, adapted from Olah (2016). These cells are repeated for each input timestep in our sequence length. The key difference between the EA LSTM and the LSTM is the separation of the static data, $\mathbf{A_n}$), from the dynamic data $\mathbf{X_{t,n}}$. In the EA LSTM, the static data is the sole input to the input gate, producing an embedding, $\mathbf{i_t}$. In both LSTM models there is a cell state $\mathbf{C_t}$, that passes from cell to cell, capable of modelling longer-term dependencies. Note that the neural network layers correspond with the weights (W), biases (b) and activation functions (σ, tanh). These operations correspond to the yellow layers in the diagram.

persist in future timesteps. In contrast, the LSTM learns to modify the input gate $\mathbf{i_t}$ based upon the meteorological forcing data ($\mathbf{X_{t,n}}$) *and* the catchment attributes ($\mathbf{A_n}$). The output of the input gate ($\mathbf{i_t}$ or $\boldsymbol{i}$) is a vector of values between 0 and 1, which is learned from data. This vector, also known as an "embedding", translates our catchment attributes into a high-dimensional

560   space that represents catchments in a manner optimised to differentiate between catchment rainfall-runoff behaviours. Kratzert et al. (2019) demonstrated how this embedding represents what the model has learned about our catchments.

For the sake of clarity, it is important to note that both models receive the same information. The LSTM still receives the static catchment attributes. However, rather than affecting only the input gate, the static data can influence all gates, since they are appended to a vector of dynamic inputs ($[\mathbf{X_{t,n}}, \mathbf{A_n}]$) and so the same information is given to the LSTM at each timestep.

565   The static attributes are used by the LSTM in the same way as the dynamic data. This offers extra flexibility for the LSTM compared with the EA LSTM, since the LSTM is able to modify the input gate based on information from time-varying data, whereas the EA LSTM is not. We are using the static nature of the data as a constraint on the EA LSTM to reflect the nature of the input data (separated into static and dynamic inputs - see Fig. A1).

Both models have a final layer, a fully connected linear layer, which transforms the $\mathbf{h_t}$ vector into a single discharge predic-

570   tion, $\mathbf{\hat{y}_{t,n}}$.

Appendix B: Comparison of the Train and Test Periods

The calibration (train) period and the evaluation (test) period are similar in terms of their predictability, although the evaluation period was slightly less predictable, as can be seen in the shifting of the two baseline model distributions towards lower NSE values (see Fig. B1). We used two baseline models to test how "predictable" the catchment hydrographs are in these two time periods. Climatology makes a prediction based on the mean discharge for that day of the year. Persistence is equivalent to predicting yesterday's value today, predicting the future will be the same as the past. Fig. B1 shows that the processes are largely stationary, and the period we use for calibration is similar to the period we use for evaluation. Indeed, the period we use for calibration is slightly easier to predict than the test period, since the benchmark models perform better, i.e. the distribution of catchment NSE scores is shifted towards higher NSE scores during the train period. Furthermore, the conditions for precipitation, PET, temperature and specific discharge are very similar between the train and test period. The temperatures have warmed slightly and there are slightly more days with zero precipitation, however, it is unlikely that such small changes have impacted the ability of the DL model to generalize. Discharge has risen slightly in the period of interest, across Great Britain.
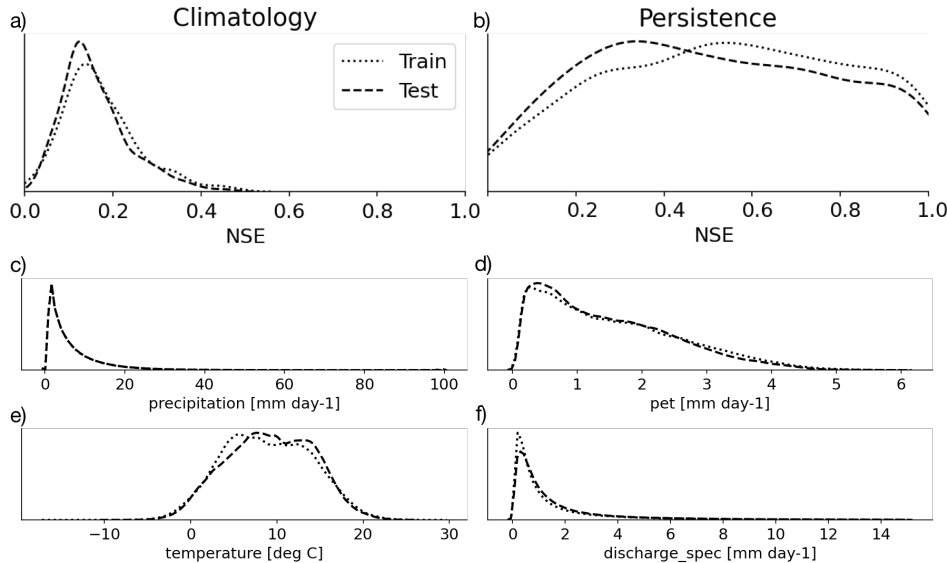
Figure B1. Kernel Density Estimates (KDE) of NSE scores for two baseline models (above), Climatology (a) (calculated as the mean discharge for that day-of-year for each site) and Persistence (b) (calculated as the discharge shifted one day into the future, so yesterdays discharge is a prediction of today). Below, Kernel Density Estimates are provided for hydro-meteorological variables, precipitation (c), potential evaporation (pet) (d), temperature (e) and specific discharge (f) in the training period (1980–1997, dotted line) and the test period (1998–2008, dashed line). Climatology represents the mean conditions for that day of the year. Persistence reflects predicting yesterday's values today, i.e. predicting no change from yesterday. These give an overview of how "predictable" a time period is, since if these baseline models perform well, it will be easier to score at least as well as the baseline.

Appendix C: Model Hydrographs

585   We illustrate the model predictions by showing the hydrographs for three stations from the Thames, the Severn and the Tay, as
the largest rivers having at least part of their catchment in England, Wales and Scotland respectively.
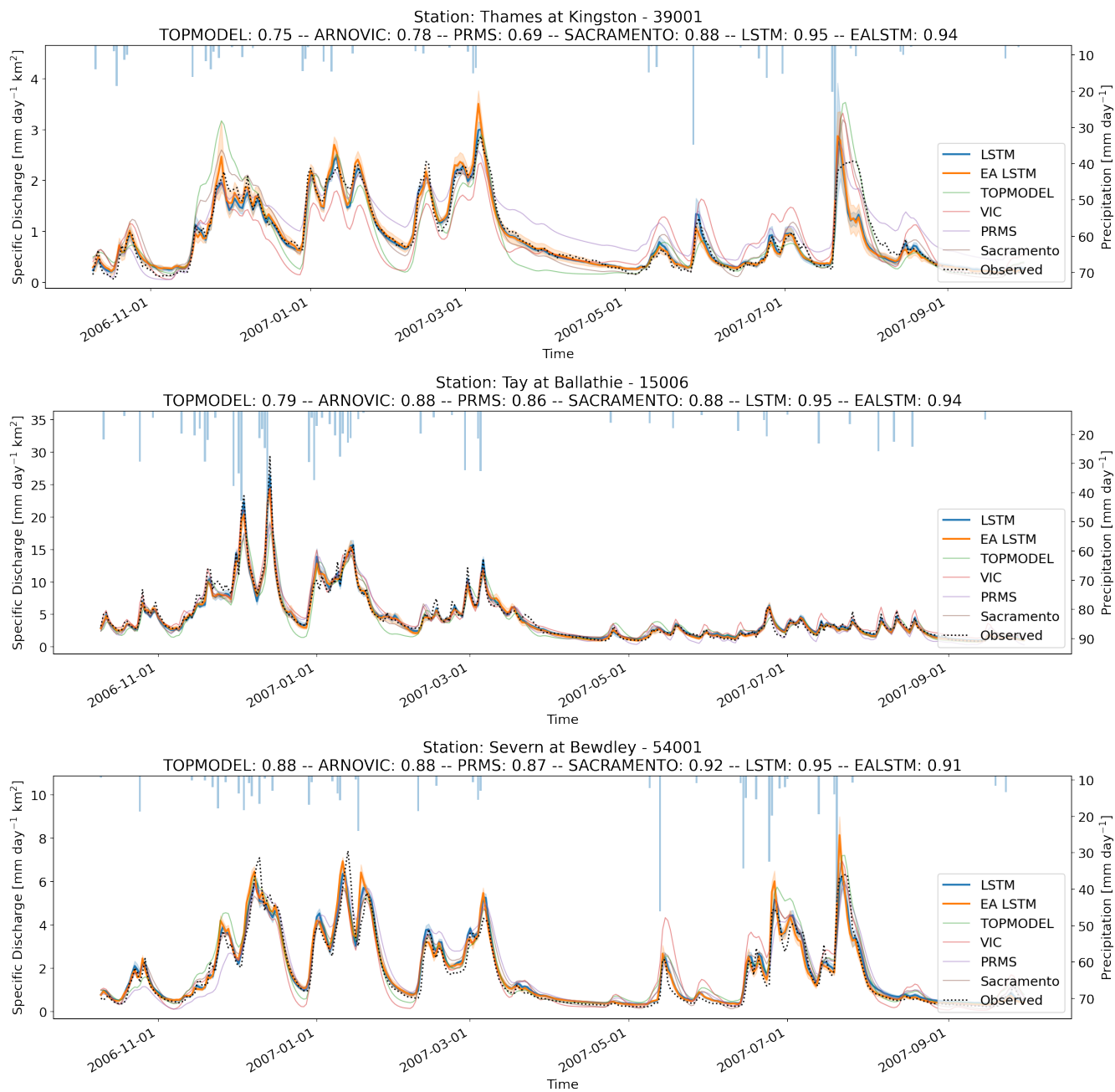
Figure C1. Hydrographs for the Thames at Kingston (Station 39001), the Tay at Ballathie (Station 15006) and the Severn at Bewdley (Station 54001), for the hydrological year from October 2006 – September 2007. The model performances displayed in the header reflect the performance of each model on the entire test period (1998–2008), not just the displayed period. The observed discharge, from (Coxon et al., 2020a), is shown as a dotted black line. The bars reflect catchment averaged precipitation with the axis shown on the right side. The LSTM and EA LSTM simulations are shown in blue and orange respectively. Conceptual model simulations for Sacramento (brown), VIC (red), PRMS (purple) and TOPMODEL (green) are taken from published timeseries from Lane et al. (2019).

Appendix D: Model Uncertainty

Uncertainty is present in all rainfall-runoff models. Model uncertainty has three main sources: (i) uncertainties in the observed data used to calibrate (train) hydrological models (McMillan et al., 2010); (ii) uncertainties in model structure (Fenicia et al., 2014; Krueger et al., 2010); and (iii) uncertainties in model parameters (Beven and Freer, 2001; Gupta et al., 2009; Arsenault et al., 2014). Parameter uncertainty can be evaluated by using an uncertainty evaluation framework (Beven and Binley, 2014), often involving a sampling strategy. Model structural uncertainty is often estimated within multi-model frameworks, such as the Modular Modelling System (Leavesley et al., 1996) or the Framework for Understanding Structural Errors (FUSE) (Clark et al., 2008). Uncertainties in observations can be estimated and accounted for by using multiple forcing products (Kratzert et al., 2021) or by resampling the input data. This study addresses predictive uncertainty in the LSTM-based models by using an ensemble of 8 LSTM models trained with different random seeds, representing different starting conditions for the training process.

The results in the main text, unless otherwise specified, show diagnostic scores given the ensemble mean discharge. Here, we discuss the ensemble range and the uncertainty that this represents. The ensemble is produced by different random seeds, and therefore different starting parameters used during the training process. The mean catchment ensemble variability is 0.16 mm^3 day^{-1}. The median is 0.12 mm^3 day^{-1}. However, model uncertainties and their relationship with catchment attributes are in accordance with our hydrological intuition. For example, we see increasing uncertainty at increased streamflow (Fig. D1). Furthermore, by normalising for mean catchment discharge we can calculate ensemble standard deviation as a ratio of total discharge. This coefficient of variability is greatest in the South East of England (Fig. D2). A more principled treatment of uncertainty, which benchmarks various methods for using DL models to directly simulate a distribution can be found in Klotz et al. (2020).
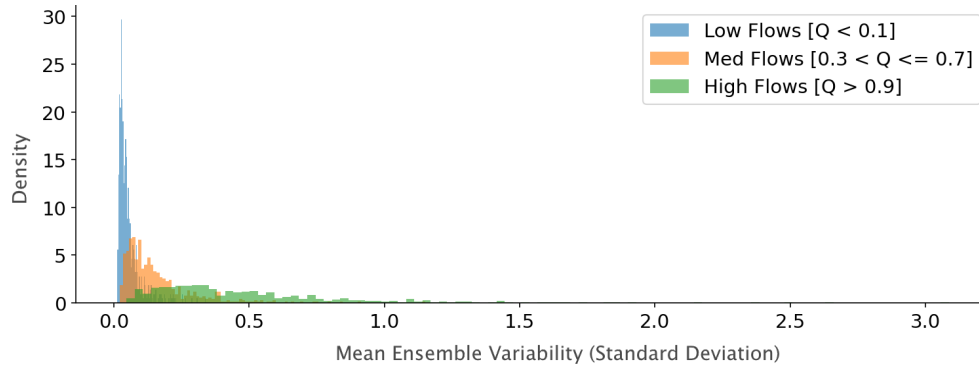
Figure D1. Histogram of raw station averaged variability (standard deviation) across ensemble members. The blue histogram reflects the variability in simulations where observed discharge is lower than the 10th percentile ($y\_true_{t,n} Q_n^{0.1}$). The green histogram shows variability for only those times where observed discharge is greater than the 90th percentile ($y\_true_{t,n} Q_n^{0.9}$). The orange histogram shows variability for all times when the observed discharge is between the 30th and 70th percentile ($Q_n^{0.3} y\_true_{t,n} Q_n^{0.7}$.)
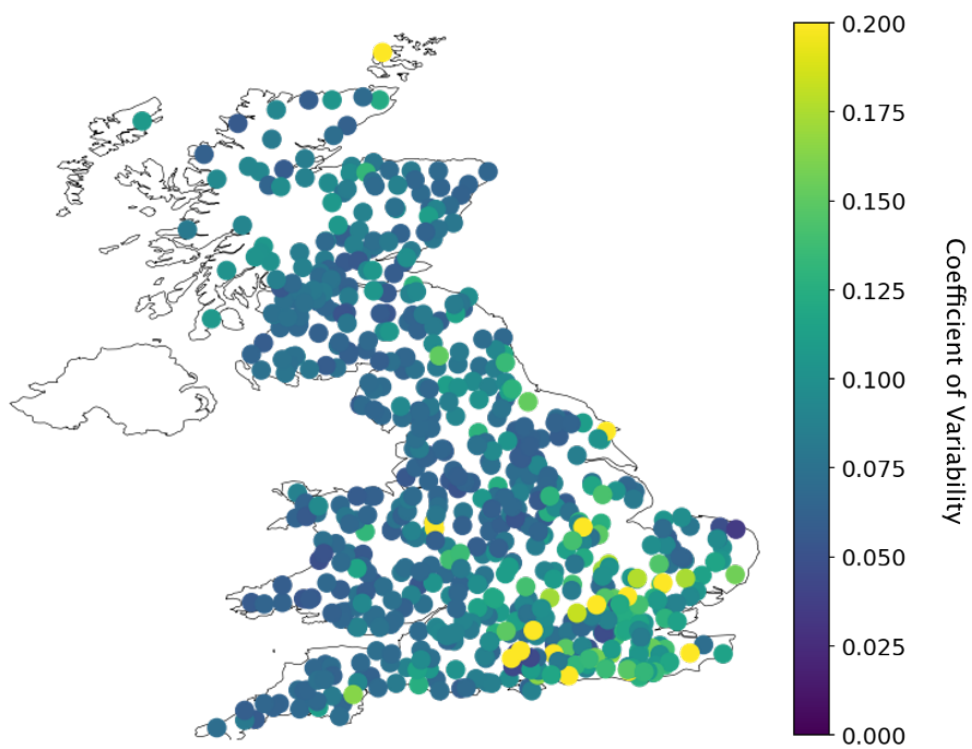
Figure D2. Spatial Patterns of normalised catchment averaged variability (standard deviation) of ensemble predictions. Brighter colours reflect greater variability across members of the ensemble of LSTMs.

Appendix E: Spatial Performances of Error Metrics
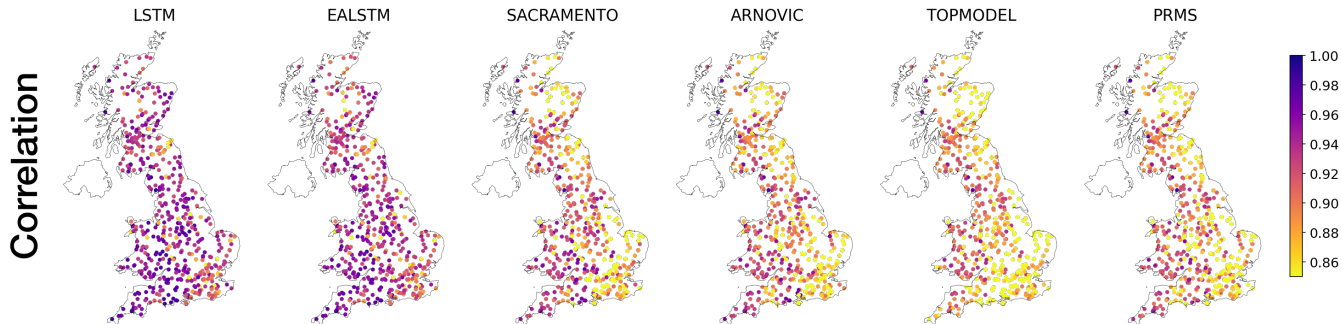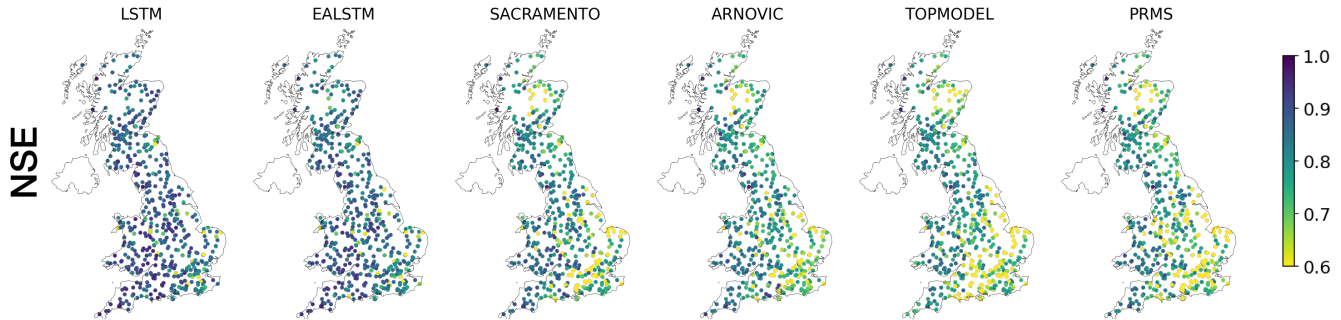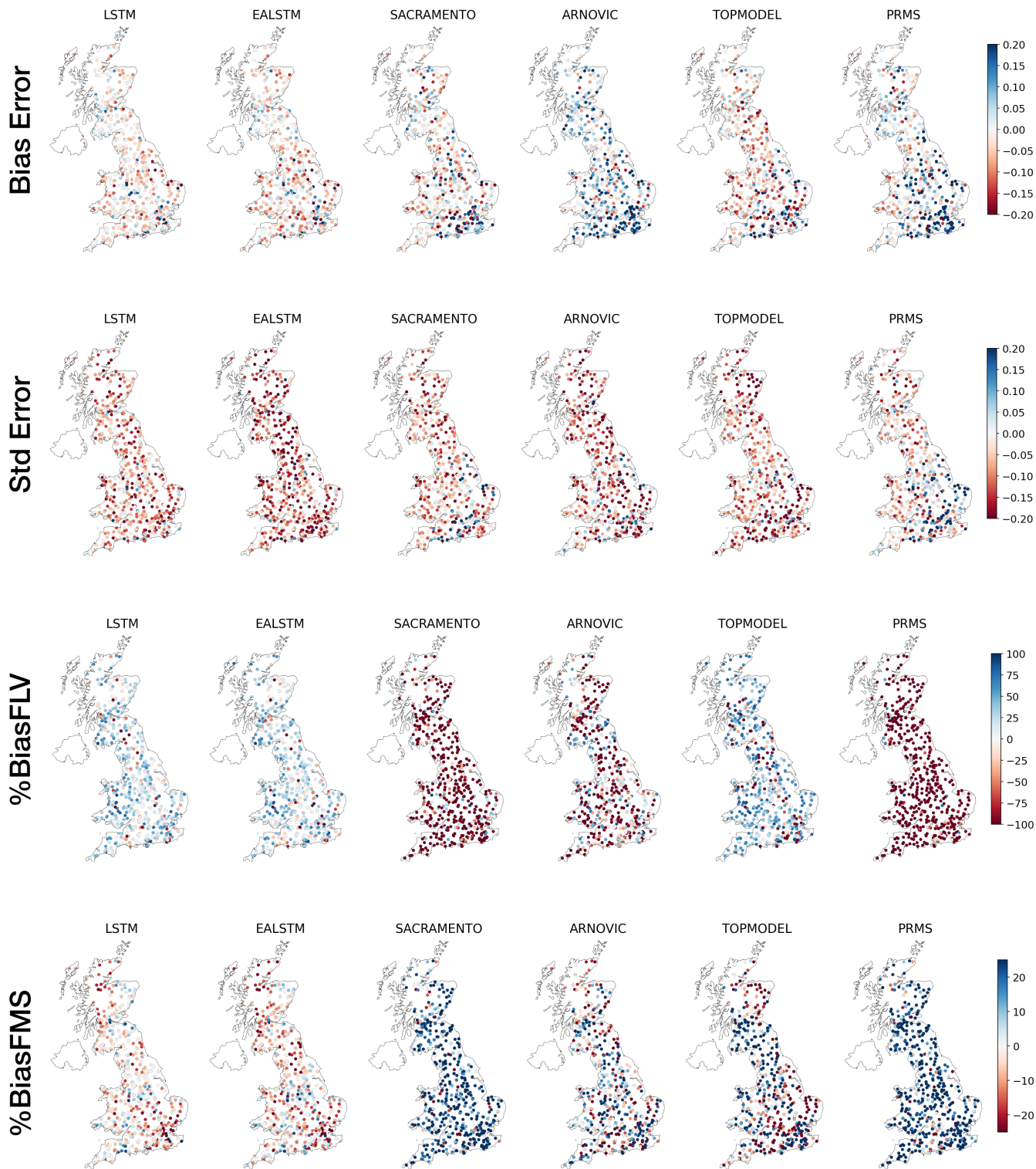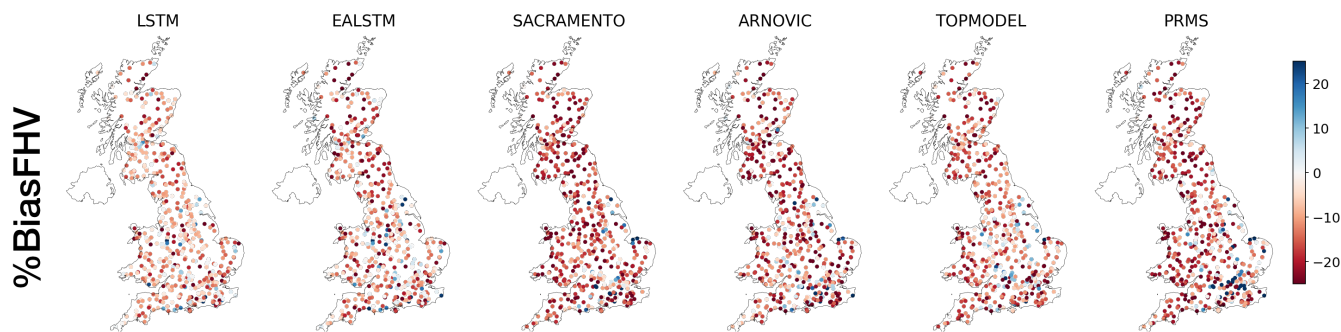
Figure E1. Spatial Patterns of different performance metrics. Each point is a single station-gauge, and the point is coloured according to the performance metric. For performance metrics with a diverging score (above and below an optimum, e.g. Bias Error) more intense colours represent worse performance. Red represents an under-prediction, blue an over-prediction. For scores which are increasing (e.g. NSE, Correlation), darker colours reflect improved performance.
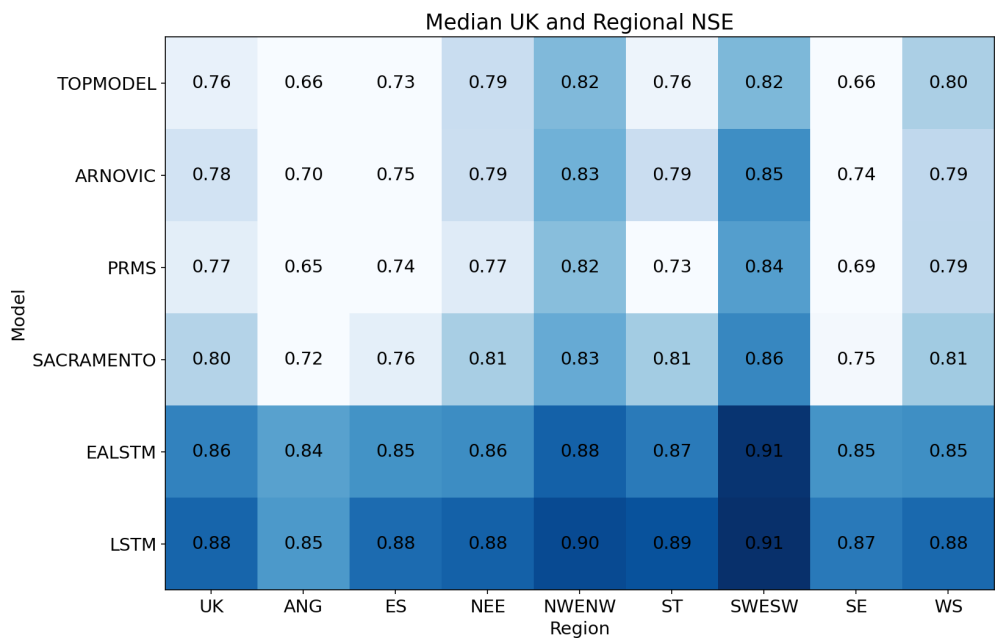
Figure E2. Median NSE scores for eight Great Britain river basin regions. The regions are based on the UKCP09 river basins (mur) aggregated from 21 river basin districts to eight regions. The leftmost column is the median score for all GB catchments, which is the same as in Table 3. It is included here for reference.

Author contributions. TL designed and conducted all experiments and analysed results with advice from SD, LS, and SR. MB performed preliminary geospatial analysis; GC guided the water balance analysis. All authors discussed and assisted with interpretation of the results and contributed to the manuscript.

Competing interests. The authors declare that they have no conflict of interest.

Acknowledgements. The authors would like to thank the teams responsible for releasing CAMELS GB (Coxon et al., 2020b), the FUSE benchmarking study (Lane et al., 2019) and the authors and maintainers of the neuralhydrology codebase for training machine learning models for rainfall-runoff modelling. TL is supported by the NPIF award NE/L002612/1; MB is supported by NERC DTP studentship NE/L002612/1, and BA is supported by the Clarendon Scholarship. SD is supported by NERC grant NE/S017380/1. We thank three anonymous reviewers for comments which have substantially improved this manuscript.

610

615

References

Addor, N. and Melsen, L.: Legacy, rather than adequacy, drives the selection of hydrological models, Water Resources Research, 55, 378–390, 2019.

Addor, N., Newman, A. J., Mizukami, N., and Clark, M. P.: The CAMELS data set: catchment attributes and meteorology for large-sample studies, Hydrology and Earth System Sciences (HESS), 21, 5293–5313, 2017.

Alvarez-Garreton, C., Mendoza, P. A., Boisier, J. P., Addor, N., Galleguillos, M., Zambrano-Bigiarini, M., Lara, A., Cortes, G., Garreaud, R., McPhee, J., et al.: The CAMELS-CL dataset: catchment attributes and meteorology for large sample studies-Chile dataset, Hydrology and Earth System Sciences, 22, 5817–5846, 2018.

Arsenault, R., Poulin, A., Côté, P., and Brissette, F.: Comparison of stochastic optimization algorithms in hydrological model calibration, Journal of Hydrologic Engineering, 19, 1374–1384, 2014.

Bengio, Y., Simard, P., and Frasconi, P.: Learning Long-Term Dependencies with Gradient Descent is Difficult, IEEE Transactions on Neural Networks, 5, 157–166, 1994.

Beven, K.: A manifesto for the equifinality thesis, Journal of hydrology, 320, 18–36, 2006a.

Beven, K.: Searching for the Holy Grail of scientific hydrology: Q t=(S, R, Δt) A as closure, Hydrology and earth system sciences, 10, 609–618, 2006b.

Beven, K.: Deep learning, hydrological processes and the uniqueness of place, Hydrological Processes, 34, 3608–3613, https://doi.org/10.1002/hyp.13805, 2020.

Beven, K. and Binley, A.: GLUE: 20 years on, Hydrological processes, 28, 5897–5918, 2014.

Beven, K. and Freer, J.: Equifinality, data assimilation, and uncertainty estimation in mechanistic modelling of complex environmental systems using the GLUE methodology, Journal of hydrology, 249, 11–29, 2001.

Beven, K. J.: Rainfall-runoff modelling: the primer, John Wiley & Sons, 2011.

Beven, K. J. and Kirkby, M. J.: A physically based, variable contributing area model of basin hydrology/Un modèle à base physique de zone d'appel variable de l'hydrologie du bassin versant, Hydrological Sciences Journal, 24, 43–69, 1979.

Birkinshaw, S. J., James, P., and Ewen, J.: Graphical user interface for rapid set-up of SHETRAN physically-based river catchment model, Environmental Modelling & Software, 25, 609–610, 2010.

Booker, D. and Woods, R.: Comparing and combining physically-based and empirically-based approaches for estimating the hydrology of ungauged catchments, Journal of Hydrology, 508, 227–239, 2014.

Bracken, L. J. and Croke, J.: The concept of hydrological connectivity and its contribution to understanding runoff-dominated geomorphic systems, Hydrological Processes, 21, 1749–1763, https://doi.org/https://doi.org/10.1002/hyp.6313, https://onlinelibrary.wiley.com/doi/abs/10.1002/hyp.6313, 2007.

Burnash, R., Ferral, R., and McGuire, R.: A generalised streamflow simulation system–conceptual modelling for digital computers. Joint Federal and State River Forecast Center, Tech. rep., Sacramento, Technical Report, 1973.

Centre for Ecology and Hydrology: https://nrfa.ceh.ac.uk/, 2016.

Chadalawada, J., Herath, H., and Babovic, V.: Hydrologically Informed Machine Learning for Rainfall-Runoff Modeling: A Genetic Programming-Based Toolkit for Automatic Model Induction, Water Resources Research, 56, e2019WR026 933, 2020.

Chagas, V. B., Chaffe, P. L., Addor, N., Fan, F. M., Fleischmann, A. S., Paiva, R. C., and Siqueira, V. A.: CAMELS-BR: hydrometeorological time series and landscape attributes for 897 catchments in Brazil, Earth System Science Data, 12, 2075–2096, 2020.

655 Clark, M. and Khatami, S.: The evolution of Water Resources Research, Eos, https://doi.org/10.1029/2021EO155644, 2021.

Clark, M. P., Slater, A. G., Rupp, D. E., Woods, R. A., Vrugt, J. A., Gupta, H. V., Wagener, T., and Hay, L. E.: Framework for Understanding Structural Errors (FUSE): A modular framework to diagnose differences between hydrological models, Water Resources Research, 44, 2008.

Coxon, G., Addor, N., Bloomfield, J., Freer, J., Fry, M., Hannaford, J., Howden, N., Lane, R., Lewis, M., Robinson, E., Wagener, T.,
660 and Woods, R.: Catchment attributes and hydro-meteorological timeseries for 671 catchments across Great Britain (CAMELS-GB), https://doi.org/10.5285/8344e4f3-d2ea-44f5-8afa-86d2987543a9, https://doi.org/10.5285/8344e4f3-d2ea-44f5-8afa-86d2987543a9, 2020a.

Coxon, G., Addor, N., Bloomfield, J. P., Freer, J., Fry, M., Hannaford, J., Howden, N. J., Lane, R., Lewis, M., Robinson, E. L., et al.: CAMELS-GB: Hydrometeorological time series and landscape attributes for 671 catchments in Great Britain, Earth System Science Data
665 Discussions, pp. 1–34, 2020b.

Crooks, S. M., Kay, A. L., Davies, H. N., and Bell, V. A.: From Catchment to National Scale Rainfall-Runoff Modelling: Demonstration of a Hydrological Modelling Framework, Hydrology, 1, 63–88, https://doi.org/10.3390/hydrology1010063, https://www.mdpi.com/2306-5338/1/1/63, 2014.

Daniell, T.: Neural networks. Applications in hydrology and water resources engineering, in: National Conference Publication- Institute of
670 Engineers. Australia, 1991.

Dawson, C. W. and Wilby, R.: An artificial neural network approach to rainfall-runoff modelling, Hydrological Sciences Journal, 43, 47–66, 1998.

Duan, S., Ullrich, P., and Shu, L.: Using Convolutional Neural Networks for Streamflow Projection in California, Front. Water 2: 28. doi: 10.3389/frwa, 2020.

675 Elshorbagy, A., Corzo, G., Srinivasulu, S., and Solomatine, D.: Experimental investigation of the predictive capabilities of data driven modeling techniques in hydrology-Part 2: Application, Hydrology and Earth System Sciences, 14, 1943–1961, 2010.

Fang, K., Pan, M., and Shen, C.: The value of SMAP for long-term soil moisture estimation with the help of deep learning, IEEE Transactions on Geoscience and Remote Sensing, 57, 2221–2233, 2018.

Fang, K., Kifer, D., Lawson, K., and Shen, C.: Evaluating the Potential and Challenges of an Uncertainty Quantification Method for Long
680 Short-Term Memory Models for Soil Moisture Predictions, Water Resources Research, 56, e2020WR028 095, 2020.

Feng, D., Fang, K., and Shen, C.: Enhancing streamflow forecast and extracting insights using long-short term memory networks with data integration at continental scales, Water Resources Research, 56, e2019WR026 793, 2020.

Fenicia, F., Kavetski, D., Savenije, H. H., Clark, M. P., Schoups, G., Pfister, L., and Freer, J.: Catchment properties, function, and conceptual model representation: is there a correspondence?, Hydrological Processes, 28, 2451–2467, 2014.

685 Gauch, M., Kratzert, F., Klotz, D., Nearing, G., Lin, J., and Hochreiter, S.: Rainfall–runoff prediction at multiple timescales with a single Long Short-Term Memory network, Hydrology and Earth System Sciences, 25, 2045–2062, 2021a.

Gauch, M., Mai, J., and Lin, J.: The proper care and feeding of CAMELS: How limited training data affects streamflow prediction, Environmental Modelling & Software, 135, 104 926, 2021b.

Gupta, H. V., Sorooshian, S., and Yapo, P. O.: Toward improved calibration of hydrologic models: Multiple and noncommensu-
690 rable measures of information, Water Resources Research, 34, 751–763, https://doi.org/10.1029/97WR03495, https://agupubs.

onlinelibrary.wiley.com/doi/full/10.1029/97WR03495https://agupubs.onlinelibrary.wiley.com/doi/abs/10.1029/97WR03495https: //agupubs.onlinelibrary.wiley.com/doi/10.1029/97WR03495, 1998.

Gupta, H. V., Kling, H., Yilmaz, K. K., and Martinez, G. F.: Decomposition of the mean squared error and NSE performance criteria: Implications for improving hydrological modelling, Journal of hydrology (Amsterdam), 377, 80–91, 2009.

695 Gupta, H. V., Perrin, C., Bloschl, G., Montanari, A., Kumar, R., Clark, M., and Andréassian, V.: Large-sample hydrology: a need to balance depth with breadth, 2014.

Halff, A. H., Halff, H. M., and Azmoodeh, M.: Predicting runoff from rainfall using neural networks, in: Engineering hydrology, pp. 760–765, ASCE, 1993.

Herath, H. M. V. V., Chadalawada, J., and Babovic, V.: Hydrologically Informed Machine Learning for Rainfall-Runoff Modelling: Towards

700 Distributed Modelling, Hydrology and Earth System Sciences Discussions, pp. 1–42, 2020.

Hochreiter, S.: Untersuchungen zu dynamischen neuronalen Netzen, Diploma, Technische Universität München, 91, 1991.

Hochreiter, S., Bengio, Y., Frasconi, P., Schmidhuber, J., et al.: Gradient Flow in Recurrent Nets: The Difficulty of Learning Long-Term Dependencies, 2001.

Hoedt, P.-J., Kratzert, F., Klotz, D., Halmich, C., Holzleitner, M., Nearing, G., Hochreiter, S., and Klambauer, G.: MC-LSTM: Mass-

705 Conserving LSTM, 2021.

Huntingford, C., Jeffers, E. S., Bonsall, M. B., Christensen, H. M., Lees, T., and Yang, H.: Machine learning and artificial intelligence to aid climate change research and preparedness, Environmental Research Letters, 14, 124 007, 2019.

Jiang, S., Zheng, Y., and Solomatine, D.: Improving AI system awareness of geoscience knowledge: Symbiotic integration of physical approaches and deep learning, Geophysical Research Letters, 47, e2020GL088 229, 2020.

710 Kingma, D. P. and Ba, J.: Adam: A method for stochastic optimization, arXiv preprint arXiv:1412.6980, 2014.

Klotz, D., Kratzert, F., Gauch, M., Sampson, A. K., Klambauer, G., Hochreiter, S., and Nearing, G.: Uncertainty Estimation with Deep Learning for Rainfall-Runoff Modelling, arXiv preprint arXiv:2012.14295, 2020.

Knoben, W. J., Freer, J. E., Fowler, K. J., Peel, M. C., and Woods, R. A.: Modular Assessment of Rainfall-Runoff Models Toolbox (MAR-RMoT) v1. 2: an open-source, extendable framework providing implementations of 46 conceptual hydrologic models as continuous

715 state-space formulations, 2019.

Kratzert, F., Klotz, D., Brenner, C., Schulz, K., and Herrnegger, M.: Rainfall–runoff modelling using Long Short-Term Memory (LSTM) networks, Hydrology and Earth System Sciences, 22, 6005–6022, https://doi.org/10.5194/hess-22-6005-2018, https://hess.copernicus.org/ articles/22/6005/2018/, 2018.

Kratzert, F., Klotz, D., Shalev, G., Klambauer, G., Hochreiter, S., and Nearing, G.: Towards learning universal, regional, and local hy-

720 drological behaviors via machine learning applied to large-sample datasets, Hydrology and Earth System Sciences, 23, 5089–5110, https://doi.org/10.5194/hess-23-5089-2019, https://hess.copernicus.org/articles/23/5089/2019/, 2019.

Kratzert, F., Klotz, D., Hochreiter, S., and Nearing, G. S.: A note on leveraging synergy in multiple meteorological data sets with deep learning for rainfall–runoff modeling, Hydrology and Earth System Sciences, 25, 2685–2703, 2021.

Krueger, T., Freer, J., Quinton, J. N., Macleod, C. J., Bilotta, G. S., Brazier, R. E., Butler, P., and Haygarth, P. M.: Ensemble evaluation of

725 hydrological model hypotheses, Water Resources Research, 46, 2010.

Lane, R. A., Coxon, G., Freer, J. E., Wagener, T., Johnes, P. J., Bloomfield, J. P., Greene, S., Macleod, C. J., and Reaney, S. M.: Benchmarking the predictive capability of hydrological models for river flow and flood peak predictions across over 1000 catchments in Great Britain, Hydrology and Earth System Sciences, 23, 4011–4032, 2019.

Le, X.-H., Ho, H. V., Lee, G., and Jung, S.: Application of long short-term memory (LSTM) neural network for flood forecasting, Water, 11, 1387, 2019.

Leavesley, G., Lichty, R., Troutman, B., and Saindon, L.: Precipitation-runoff modelling system: user's manual. Report 83–4238, US Geological Survey Water Resources Investigations, 207, 1983.

Leavesley, G., Markstrom, S., Brewer, M., and Viger, R.: The modular modeling system (MMS)—The physical process modeling component of a database-centered decision support system for water and power management, Water, Air, & Soil Pollution, 90, 303–311, 1996.

Liang, X.: A two-layer variable infiltration capacity land surface representation for general circulation models., PhD Thesis, 1994.

Maxwell, R. M., Kollet, S. J., Smith, S. G., Woodward, C. S., Falgout, R. D., Ferguson, I. M., Baldwin, C., Bosl, W. J., Hornung, R., and Ashby, S.: ParFlow user's manual, International Ground Water Modeling Center Report GWMI, 1, 129, 2009.

McMillan, H., Freer, J., Pappenberger, F., Krueger, T., and Clark, M.: Impacts of uncertain river flow data on rainfall-runoff model calibration and discharge predictions, Hydrological Processes: An International Journal, 24, 1270–1284, 2010.

Nash, J. E. and Sutcliffe, J. V.: River flow forecasting through conceptual models part I—A discussion of principles, Journal of hydrology, 10, 282–290, 1970.

Nearing, G., Kratzert, F., Sampson, A. K., Pelissier, C. S., Klotz, D., Frame, J., Prieto, C., and Gupta, H.: What Role Does Hydrological Science Play in the Age of Machine Learning?, https://doi.org/10.31223/osf.io/3sx6g, eartharxiv.org/3sx6g, 2020a.

Nearing, G. S., Ruddell, B. L., Bennett, A. R., Prieto, C., and Gupta, H. V.: Does Information Theory Provide a New Paradigm for Earth Science? Hypothesis Testing, Water Resources Research, 56, e2019WR024 918, 2020b.

Nearing, G. S., Ruddell, B. L., Bennett, A. R., Prieto, C., and Gupta, H. V.: Does information theory provide a new paradigm for earth science? Hypothesis testing, Water Resources Research, 56, 2020c.

Nourani, V., Baghanam, A. H., Adamowski, J., and Kisi, O.: Applications of hybrid wavelet–artificial intelligence models in hydrology: a review, Journal of Hydrology, 514, 358–377, 2014.

Olah, C.: Understanding LSTM Networks – colah's blog, http://colah.github.io/posts/2015-08-Understanding-LSTMs/, 2016.

Peel, M. C. and McMahon, T. A.: Historical development of rainfall-runoff modeling, Wiley Interdisciplinary Reviews: Water, 7, e1471, 2020.

Reichstein, M., Camps-Valls, G., Stevens, B., Jung, M., Denzler, J., Carvalhais, N., and Prabhat: Deep learning and process understanding for data-driven Earth system science, Nature, 566, 195–204, https://doi.org/10.1038/s41586-019-0912-1, https://www.nature.com/articles/s41586-019-0912-1, 2019.

Robinson, E., Blyth, E., Clark, D., Comyn-Platt, E., Finch, J., and Rudd, A.: Climate Hydrology and Ecology Research Support System Meteorology Dataset for Great Britain (1961-2015) [CHESS-met] v1.2, https://doi.org/10.5285/b745e7b1-626c-4ccc-ac27-56582e77b900, https://doi.org/10.5285/b745e7b1-626c-4ccc-ac27-56582e77b900, 2017.

Shen, C.: A Transdisciplinary Review of Deep Learning Research and Its Relevance for Water Resources Scientists, Water Resources Research, 54, 8558–8593, https://doi.org/10.1029/2018WR022643, https://agupubs.onlinelibrary.wiley.com/doi/abs/10.1029/2018WR022643, 2018.

Shen, C., Laloy, E., Albert, A., Chang, F.-J., Elshorbagy, A., Ganguly, S., Hsu, K.-l., Kifer, D., Fang, Z., Fang, K., et al.: HESS Opinions: Deep learning as a promising avenue toward knowledge discovery in water sciences, Hydrology and Earth System Sciences Discussions, 2018, 1–21, 2018.

Srivastava, N., Hinton, G., Krizhevsky, A., Sutskever, I., and Salakhutdinov, R.: Dropout: A Simple Way to Prevent Neural Networks from Overfitting, Journal of Machine Learning Research, 15, 1929–1958, http://jmlr.org/papers/v15/srivastava14a.html, 2014.

Tanguy, M.;Dixon, H. I. D. G. V. D. J.: Gridded estimates of daily and monthly areal rainfall for the United Kingdom (1890-2012) [CEH-GEAR], https://doi.org/10.5285/5dc179dc-f692-49ba-9326-a6893a503f6e, https://doi.org/10.5285/5dc179dc-f692-49ba-9326-a6893a503f6e, 2014.

770   van Meerveld, H. J. I., Kirchner, J. W., Vis, M. J. P., Assendelft, R. S., and Seibert, J.: Expansion and contraction of the flowing stream network alter hillslope flowpath lengths and the shape of the travel time distribution, Hydrology and Earth System Sciences, 23, 4825–4834, https://doi.org/10.5194/hess-23-4825-2019, https://hess.copernicus.org/articles/23/4825/2019/, 2019.

Van Rossum, G. et al.: Python programming language., in: USENIX annual technical conference, vol. 41, p. 36, 2007.

Wilby, R., Abrahart, R., and Dawson, C.: Detection of conceptual model rainfall—runoff processes inside an artificial neural network,

775   Hydrological Sciences Journal, 48, 163–181, 2003.

Yilmaz, K. K., Gupta, H. V., and Wagener, T.: A process-based diagnostic approach to model evaluation: Application to the NWS distributed hydrologic model, Water Resources Research, 44, https://doi.org/https://doi.org/10.1029/2007WR006716, https://agupubs.onlinelibrary.wiley.com/doi/abs/10.1029/2007WR006716, 2008.

Young, P.: Data-based mechanistic modelling of environmental, ecological, economic and engineering systems, Environmental Modelling &

780   Software, 13, 105–122, 1998.

Young, P.: Top-down and data-based mechanistic modelling of rainfall–flow dynamics at the catchment scale, Hydrological processes, 17, 2195–2217, 2003.

Young, P. C. and Beven, K. J.: Data-based mechanistic modelling and the rainfall-flow non-linearity, Environmetrics, 5, 335–363, 1994.